Title: Organoid co-culture model of the cycling human endometrium in a fully-defined synthetic extracellular matrix reveals epithelial-stromal crosstalk

Authors: Juan S. Gnecco[1,2,#], Alexander Brown[1,2,#], Kira Buttrey[2], Clara Ives[1,2], Brittany A. Goods[3], Lauren Baugh[1,2], Victor Hernandez-Gordillo[2], Megan Loring[1,4], Keith Isaacson[1,4], and Linda G. Griffith*[1,2]

Affiliations: *[1]Center for Gynepathology Research, [2]Department of Biological Engineering, Massachusetts Institute of Technology, 77 Massachusetts Ave, Cambridge MA, USA 02139. [3]Thayer School of Engineering at Dartmouth College, Hanover, NH. [4]Newton Wellesley Hospital, Newton, MA USA 02115.*

 # Equal contribution

*** Corresponding author:** L.G.G. (griff@mit.edu)
Massachusetts Institute of Technology
Room 16-429
77 Massachusetts Ave
Cambridge, MA 02139
Phone: (617) 253-0013

Summary:

The human endometrium undergoes recurring cycles of growth, differentiation, and breakdown in response to sex hormones. Dysregulation of epithelial-stromal communication during hormone cycles is linked to myriad gynecological disorders for which treatments remain inadequate. Here, we describe a completely defined, synthetic extracellular matrix that enables co-culture of human endometrial epithelial and stromal cells in a manner that captures healthy and disease states across a simulated menstrual cycle. We parsed cycle-dependent endometrial integrin expression and matrix composition to define candidate cell-matrix interaction cues for inclusion in a polyethylene glycol (PEG)-based hydrogel crosslinked with matrix metalloproteinase-labile peptides. We semi-empirically screened a parameter space of biophysical and molecular features representative of the endometrium to define compositions suitable for hormone-driven expansion and differentiation of epithelial organoids, stromal cells, and co-cultures of the two cell types. Each cell type exhibited characteristic morphological and molecular responses to hormone changes when co-encapsulated in hydrogels tuned to a stiffness regime similar to the native tissue and functionalized with a collagen-derived adhesion peptide (GFOGER) and a fibronectin-derived peptide (PHSRN-K-RGD). Analysis of cell-cell crosstalk during IL-1β-induced inflammation revealed dysregulation of epithelial proliferation mediated by stromal cells. Altogether, we demonstrate the development of a fully synthetic matrix to sustain the dynamic changes of the endometrial microenvironment and support its applications to understand menstrual health and endometriotic diseases.

1. Introduction:

The endometrium is the mucosal lining of the uterus in which the establishment and maintenance of pregnancy occurs[1]. It is a highly dynamic tissue that undergoes spatial and temporal changes in response to endocrine signaling by the ovarian sex hormones estradiol (E_2) and progesterone (P4). Cyclical changes in these hormones dictate the timing and functional capabilities of the endometrium to support nidation by driving cell-specific morphological and biochemical processes[2]. Histologically, the endometrium is primarily composed of the hormone-responsive epithelium and specialized reticular fibroblasts (stromal cells) embedded in a dynamic extracellular matrix (ECM).[1,3,4] Endocrine-mediated reproductive function is mediated through both direct and indirect mechanisms governed by the crosstalk between these cell populations.[5–7] The idealized 28-day human menstrual cycle is characterized by three distinct phases in which the endometrium undergoes E_2-mediated tissue regeneration (the 'proliferative phase') followed by a 14-day P4-dominant phase (the 'secretory phase') that governs the differentiation processes necessary for the successful establishment of pregnancy (Fig 1A). In the absence of embryo implantation, a sharp withdrawal of hormones triggers a cascade of inflammatory processes that result in the shedding of the endometrial tissue (the 'menstrual phase') after which the cycle initiates again.[1,3] Despite the fundamental roles E_2 and P4 play in maintaining reproductive functions, a thorough understanding of the cellular mechanisms driving these processes remains elusive due in part to a lack of physiological models that recapitulate the complex multi-cellular human condition.[1,8]

Experimental models capable of recapitulating epithelial-stromal crosstalk are necessary to understand human reproductive physiology and pathology. Endometrial stromal cells (ESCs) are historically the most utilized primary cell type for experimentation in reproductive biology due to their ability to be cultured and expanded *in vitro*. Recently, protocols to expand and culture primary endometrial epithelial cells as endometrial epithelial organoids (EEOs) have transformed the experimental landscape for *in vitro* analysis of endometrial behavior.[9,10] Organoids are self-organizing 3D cell structures that retain many physiologically relevant and functional features of their native tissues of origin.[11] Thus, EEOs provide opportunities to investigate human reproductive function, understand disease pathogenesis[12], and test therapeutic compounds for clinical applications.[9,10] EEOs are typically generated from isolated primary endometrial glands embedded in Matrigel, a complex, murine tumor-derived ECM primarily comprising heterogenous basement membrane (BM) proteins and growth factors (GFs), together with a defined culture medium designed to enrich the expansion of the stem/progenitor compartment.[13,14] Cultured continuously in Matrigel, clonally-generated EEOs

retain columnar epithelial architecture of the native tissue and form polarized cyst-like structures that are genomically stable, hormone-responsive, and cell-heterogenous.[9,10,15] However, the reliance on Matrigel to culture organoids presents a critical obstacle for numerous experimental, analytical, and therapeutic applications for dynamic and hormone-sensitive tissues such as the endometrium.[16,17] Matrigel's inherent lot-to-lot variability, poorly-defined molecular composition, limited biophysical properties, and poor suitability for co-culture of epithelia with stromal cells have driven efforts to develop synthetic (or semi-synthetic) ECMs that are fully defined, modular, and tunable.[12,18–26]

Although endometrial epithelia and stroma are often co-cultured in naturally-derived ECM hydrogels[27–29], these models are limited by rapid ECM breakdown, which ultimately leads to highly abbreviated experimental conditions and limited control over the biophysical and molecular ECM compositions that can reliably support the morphogenic and functional behavior of multiple cell types. Recently, the development of fully or semi-synthetic ECMs to culture enteric organoids were reported for both murine[23,30] and human[17,21,26,30] tissues. We have previously demonstrated that poly(ethylene glycol) (PEG)-based hydrogel systems can be applied to model some aspects of the endometrial mucosal barrier,[25] and developed a completely synthetic hydrogel formulation for the culture, differentiation and passaging of human intestinal enteroids that also supported culture of primary endometrial epithelial cells[26]. This synthetic ECM also supports the culture of pancreatic tumor organoids with a complex stroma.[31] Despite these advances, a fully-defined synthetic ECM that can support the long-term culture and function of multiple endometrial cell populations, especially under the dynamic conditions of hormone variation in a simulated menstrual cycle, is still an unmet need.

Inspired by cell-matrix interactions in native tissue, we designed and synthesized a synthetic ECM that targets cell-specific integrins on epithelia and stroma, supports cell-secreted ECM deposition, and mimics the biophysical properties of the endometrium in health and disease. We show that this bio-labile PEG-based synthetic ECM supports the 3D co-culture of primary human EEOs and ESCs and recapitulates characteristic phenotypic properties of the endometrial responses to sex hormone changes across a simulated 15-day menstrual cycle *in vitro*. We used this 3D co-culture model to parse stromal-epithelial crosstalk and disease-related phenotypes in response to inflammatory cues.

106

107 **2. Methods:**

108

109 ***2.1. Tissue Acquisition and Isolation of Human Endometrial Cells***

110 All participants provided informed consent in accordance with a protocol approved by the
111 Partners Human Research Committee and the Massachusetts Institute of Technology
112 Committee on the Use of Humans as Experimental Subjects (Protocol number IRB-P001994).
113 Endometrial tissue was obtained from pipelle biopsies from reproductive age women (N=18,
114 ages 18-45; Table 1) undergoing laparoscopic surgery for non-malignant gynecologic
115 indications. Study enrollment was limited to pre-menopausal women and excluded patients with
116 an irregular or ambiguous cycle, or a history of hormone use in the 3 months prior to surgery.
117 Cycle phase dating was performed as described elsewhere[3] by histological analysis (Fig S20).
118 Endometrial epithelial glands and stromal cells were isolated by enzymatic digestion and filter-
119 separated as previously described[32], resulting in ≥ 95% purity as assessed by positive staining
120 for vimentin and morphological assessment. Briefly, single stromal cells were separated from
121 intact epithelial glands fragments and cultured separately. Stromal cells were expanded in
122 traditional 2D cultures (as described below) and epithelial glands were cultured as organoids
123 using protocols adapted from Turco et al.[10] All cells were passaged a maximum of 5 times for all
124 experimental *in vitro* assessments.

125

126 ***2.2. Cell Isolation and Endometrial Organoid Generation***

127 Stromal cells were cultured and maintained in phenol red-free DMEM/F12 with 5% charcoal-
128 stripped calf serum, 1 nM 17-β estradiol (E_2, Sigma Aldrich) and 1× Pen-Strep solution (Sigma
129 Aldrich). Some cell cultures were treated with 500 nM synthetic progesterone
130 medroxyprogesterone acetate (MPA, Sigma Aldrich). Primary endometrial epithelial organoids
131 (EEOs) were generated from the primary epithelial fragments (p0) according to established
132 protocols and maintained in endometrial epithelial organoid expansion medium (EEO
133 medium).[9,33] EEO media is modified from the protocols established by Turco et al.[10] Briefly, EEO
134 media was defined as the minimal set of components needed to establish organoid cultures
135 expansion and was composed of advanced basal media cocktail[10] (ABM, 1X); rhEGF (50
136 ng/mL, Corning); rhNoggin (100 ng/mL, Peprotech); rhRspondin-1 (200 ng/mL, R&D systems);
137 rhFGF-10 (50 ng/mL, Peprotech); Estradiol (E_2, 1nM, Sigma Aldrich); Nicotinamide (1mM);
138 Insulin-Transferrin-Selenium (ITS, 1%, Invitrogen); N-Acetyl-L-Cysteine (1.25 mM); TGFB
139 pathway inhibitor (A83-01, 500 nM, Peprotech); and Rock inhibitor Y-27632, (ROCKi, 10 μM,

140 Tocris). For seeding, epithelial cells, as fragments or single cell suspensions, were embedded in
141 70% Matrigel and cultured for 6 days, with media was changed every two days (Fig S2). For
142 passaging, 6-day old organoids were incubated in Cell Recovery Solution (CRS, Gibco) for 30
143 mins at 4°C to dissolve Matrigel, then pelleted and digested with Tryp-LE supplemented with
144 1:100 DNAse (40k units, Sigma) for 15 minutes in a 37°C water bath followed by mechanical
145 dissolution to generate single cells. For expansion purposes, single epithelial cells were seeded
146 in Matrigel at a density of 1,000 cells/μL in 60μL droplets in non-tissue culture treated plates.
147 We refer to organoids generated from single cells, in regular expansion or in experiments, as
148 scEEOs. For co-culture experiments of ESC and scEEOs, ROCKi was omitted from EEO media
149 since intact organoids were utilized to establish the co-cultures. ESCs retained hormone
150 sensitivity and morphological characteristic when cultured in this EEO-based common media
151 (See Results). Due to the presence of progesterone in the N2 and B27 supplements in the
152 advanced basal media a homemade formulation of EEO media termed neutral EEO (nEEO)
153 media that omitted P4 in the supplements was also explored in some experiments. All media
154 changes for the co-cultures occurred every 3 days for up to 15 days unless noted otherwise.
155 Spent conditioned media from these cultures was collected and stored at -80°C for downstream
156 analysis.
157
158 ***2.3. PEG hydrogel materials and peptides.***
159 8-arm poly(ethylene glycol) (PEG) macromers (20 kDa) functionalized with vinyl sulfone (20 kDa
160 PEG-VS) were purchased from JenKem Technology. All peptides were custom synthesized and
161 purified (>95%) by Boston Open Labs (Cambridge, MA), GenScript (Piscataway, NJ), or CPC
162 Scientific (Sunnyvale, CA). Peptides used in these studies include: a dithiol crosslinking peptide
163 containing a matrix metalloproteinase (MMP)-sensitive substrate (Ac)GCRD-LPRTG-
164 GPQGIWGQ-DRCG(Am) (***CL-LW***); fibronectin (FN)-derived peptide containing both the
165 canonical RGD motif from the 10th FN type III domain as well as the PHSRN synergy site from
166 the 9th FN Type III repeat in a branched configuration akin to the biophysical presentation in FN,
167 (Ac)PHSRNGGGK-GGGERCG(Ac) -GGRGDSPY(Am) (***PHSRN-K-RGD***);[34–36] a Collagen I-
168 derived peptide, (Ac)GGYGGGPG(GPP)$_5$GFOGER(GPP)$_5$GPC(Am) (***GFOGER***);[21,37] a peptide
169 with affinity for sequestering cell-produced FN, (Ac)KKGCRE-TLQPVYEYMVGV(Am) (***FN-***
170 ***binder***);[38] and a peptide with affinity for sequestering the basement membrane proteins type IV
171 collagen and laminin, (Ac)GCRE-ISAFLGIPFAEPPMGPRRFLPPEPKKP(Am) (***BM-binder***).[39] All
172 peptides were reconstituted in acidic (pH 5.5) Milli-Q water (Millipore). The concentration of free
173 thiols in all peptides was determined using Ellman's reagent (Sigma Aldrich).

174

175 ***2.4. Fabrication of synthetic PEG extracellular matrix.***

176 Synthetic matrices were assembled using materials at the concentrations indicated throughout
177 the text. Briefly, 8-arm 20 kDa PEG-VS macromers were prepared in a 10 w/w% solution in ultra
178 pure water. Macromers were used at concentrations ranging from 14.4-33.6 mM VS (nominally,
179 3-7 wt%). Macromers were functionalized (fPEG-VS) via a Michael-type addition reaction with
180 the integrin (*PHSRN-K-RGS, GFOGER*) and matrix-binding (*FN-binder, BM-binder*) by adding
181 10% of the total solution volume in 10x PBS + 1M HEPES, pH 8.2, vortex-mixing, and reacting
182 at room temperature for 30 minutes. Note that lyophilized peptides containing HCl salt can be
183 very acidic in stock solutions, so the pH of the final reaction mix should be maintained at 7.8 by
184 adjusting the pH of the buffer solution. During functionalization, cells were counted and pelleted
185 at the appropriate number for the target final cell densities (10,000 ESC and 10 EEO per µL of
186 gel solution). Following functionalization, care was taken to ensure that all cell media was
187 removed without disturbing the cell pellet, and pellets were gently resuspended in fPEG-VS.
188 Upon resuspension, cross linker (CL-LW) was added to the mixture at a stoichiometric ratio of
189 0.45 thiol:VS to initiate gelation. The solution was gently mixed and plated accordingly, typically
190 in 3 µL droplets in non-tissue culture treated 96-well plates unless otherwise specified in the
191 text. Cell-fPEG-VS mixture was incubated for 25 minutes in a humidified incubator at 37°C until
192 gelation was complete.

193

194 ***2.5. Rheological characterization of hydrogels***

195 To measure bulk bio-mechanical properties of crosslinked gels, 25 µL of each gel matrix mixture
196 was loaded into a 1 mL syringe that had the tip cut off at the 0.1 mL mark. The matrix was
197 allowed to gel at 37 ºC for 25 min and then extruded from the open syringe as a cylindrical disc
198 and moved to a 24 well plate that contained 400 µL of 1X PBS. The plate was incubated for 24
199 hours in a humidified incubator at 37 ºC, 95% air, and 5% CO_2, to allow equilibrium swelling to
200 occur prior to rheological characterization. This procedure generates hydrogel discs of 1.4 mm
201 in thickness. The discs were sandwiched between an 8 mm sandblasted parallel plate geometry
202 and sandblasted base. The shear modulus was determined by performing small-strain
203 oscillatory shear measurements on an Anton Parr MCR 302 rheometer. The mechanical
204 response was recorded by performing frequency sweep measurements (0.1–10 Hz) at a
205 constant strain (0.05), at 37 °C. The elastic modulus (E) is reported as a measure of bulk matrix
206 mechanical properties derived from the recorded storage modulus (G') in the linear elastic

207 regime where: $E = 2G'(1 + \nu)$ with the assumption that ν = 0.5 for ideal elastic hydrogel
208 materials.
209
210 ***2.6. EEO generation in synthetic hydrogels***
211 Endometrial organoids were established and expanded in Matrigel according to established
212 protocols[33] with some minor modifications. Lumenized organoids with a diameter greater than
213 100 µm were harvested with cold Cell Recovery Solution (CRS, ThermoFisher). Matrigel dollops
214 were manually detached with a wide bore pipette tip, making sure to fully scrape the entire well
215 to lift off the entire gel. The dollops were resuspended in cold CRS (5mL) for at least 30 mins on
216 ice to dissolve remaining Matrigel, followed by centrifugation at 500-1000g, which resulted in a
217 clear pellet of organoids. Organoids were broken into single cell suspensions using 1mL of
218 prewarmed TrypLE Express (ThermoFisher) supplemented with DNAase (10µl, 1:100) and
219 continuous mechanical agitation until a single cell suspension of epithelial cells was observed.
220 Single cells were counted using a hemocytometer then resuspended in the functionalized PEG
221 precursor (fPEG-VS) solutions prior to the addition of the crosslinker. In parallel, single cells
222 were resuspended in Matrigel that served as an experimental control during matrix evaluation.
223 In both cases, cells were encapsulated at a density of 500 cells/µL of matrix. Cell-matrix
224 suspensions were seeded as 3 µL droplets on a non-tissue treated 96 well plate and allowed to
225 polymerize for 25 min in a humidified incubator at 37 ºC, 95% air, and 5% CO_2. Complete
226 gelation was examined visually on a test gel droplet prior to the addition of media. Gel droplets
227 were maintained in 100 µL of expansion EEO media supplemented with ROCKi (10 µM). Media
228 was changed every three days.
229
230 ***2.7. Generation of co-culture model***
231 Six-day old intact organoids (~100 µm diameter) were grown and expanded in Matrigel and
232 harvested as described above. To maintain scEEO integrity, organoids were incubated in Cell
233 Recovery Solution until Matrigel was fully dissolved. Careful resuspension of intact scEEOs in
234 DMEM/F12 was performed to prevent disrupting scEEO integrity. In parallel, donor matched
235 ESCs were expanded using traditional 2D polystyrene cell culture plates and grown to 80%
236 confluency. ESCs were lifted from 2D culture plates using trypsin (1X) and processed to
237 generate a single cell suspension. Intact scEEOs and ESCs were prepared in parallel to
238 encapsulate both cell types simultaneously and establish a co-culture in the PEG matrix
239 solution. Cells were encapsulated at a density of 10,000 ESC and 10 intact scEEOs per µL of
240 matrix. This epithelial-stromal ratio (approximately 1:1) was determined experimentally based on

241 the cell ratios used to generate established endometrial xenograft models (sub-renal capsule)
242 described elsewhere[40,41] and validated using whole-mount 3D image analysis of endometrial
243 tissue we performed (see Results). Embedded cells in fPEG-vs were seeded in 3 µL droplets
244 and allowed to polymerize as described above in non-tissue culture treated 96-well plates. Co-
245 culture was maintained in EEO media without Y-27632, a common media recipe utilized in other
246 co-culture studies[42], unless otherwise noted. Media was changed every three days and
247 maintained for up to 15 days. It was noted that some basal components of the organoid medium
248 contained P4 (N2 and B27) which may impact hormone responsive behavior, so a P4-reduced
249 'neutral' formulation of this organoid medium (nEEO medium) that completely lacked P4 was
250 tested in some co-cultures. Both media formulations were sufficient to maintain support cell
251 culture and induced hormone-mediated responses (Fig S19); however, as expected, co-cultures
252 maintained in nEEO media conferred a more robust response to progestin. Matching
253 monocultures of ESCs-only or scEEOs-only were established in parallel for some experiments.
254 Cultures were imaged daily.
255
256 ***2.8. EEO and co-culture efficiency and quantification***
257 To quantify organoid diameter and total organoid formation efficiency, single epithelial cells
258 were encapsulated in fPEG-VS hydrogels or Matrigel and cultured over 14 days. scEEO
259 formation efficiency was calculated as the percentage of organoids with a clear lumen with a
260 diameter (>100 um) relative to Matrigel. 4X brightfield (BF) z-stack images of 10-day old
261 endometrial organoids were captured using an EVOS M500 microscope (Invitrogen). The
262 images were processed in Fiji using the time lapse Gaussian-based stacker focuser plugin to
263 generate maximum intensity projections. Images were manually analyzed in Fiji to obtain a
264 diameter and organoid count distribution for each condition. Daily images of co-cultures were
265 manually curated to obtain relative growth rates of the organoids in single culture (N=3) or co-
266 culture (N=8) by measuring scEEO diameter and quantifying the daily fold change relative to
267 day 1 of culture (video 3, 4).
268
269 ***2.9. Cell viability and proliferation analysis***
270 Co-culture cell viability and cell death was measured using the LIVE/DEAD™ Cell Imaging Kit
271 (488/570) (Thermofisher Scientific) according to the manufactorers protocol. Briefly,
272 At day-15 prior to fixation, cells were incubated the reagents provided by the kit and incubated
273 at 37 ºC, 95% air, and 5% CO_2 for 20 minutes. Images were captured using Keyence BZ-X800
274 Fluorescence Microscope. Cell proliferation was assessed by EdU incorporation using the Click-

275 iT Plus EdU imaging kit with Alexa Fluor 594. All co-culture and monoculture experiments were
276 treated with EdU (5-ethynyl-2′-deoxyuridine, 20 μM) for a 24-hour incubation period at 37°C,
277 95% air, 5% CO_2 prior to fixation at day 15 of culture. Click-iT reaction cocktail was prepared as
278 described by the manufacturer (ThermoFisher Scientific). Cells were incubated for 1 hr at RT
279 protected from light and counter stained with DAPI (1 mg/mL, 1:2000). Images were captured
280 using a ZEISS confocal Laser Scanning Microscope (LSM 880) and analyzed by 3D image
281 processing was performed using the Surface and Spots function in Imaris (Bitmap) software
282 (9.6.0). At least three individual organoids were analyzed per donor, and the proliferative index
283 was measured as the number of EdU^+ positive cells per organoid surface area (mm^2). ESC
284 proliferative index was calculated as the EdU^+ cells relative to the total number of DAPI stained
285 nuclei.
286
287 ***2.10. RNA isolation for quantitative real time PCR (qPCR) and bulk RNA-seq.***
288 ESCs and intact scEEOs cultured in Matrigel or synthetic hydrogels were used for molecular
289 analysis. After 14 days of culture, intact scsEEOs were released from Matrigel and the synthetic
290 ECM, using Cell Recovery Solution, or recombinant Sortase, respectively. Intact scEEO-only
291 cultures, ESC-only cultures, or co-cultures were pelleted, resuspended in TRIzol reagent
292 (ThermoFisher Scientific), and then stored at -80°C until processing. RNA was extracted using
293 the Directzol RNA Mini-Prep kit (Zymo Research) per the manufacturer's protocols with the
294 inclusion of an on-column DNase step using the PureLink DNase Set (ThermoFisher Scientific).
295 At least eight replicates (3 μl droplets) were pooled together to obtain sufficient RNA. cDNA was
296 synthesized from ~1 μg of total RNA using the High-Capacity RNA-to-cDNA Kit (ThermoFisher
297 Scientific, 4387406) per manufacturer's protocols. TaqMan Fast Advanced Master Mix
298 (ThermoFisher Scientific) was used in congruence with the cell-specific probes for qPCR. Gene
299 expression was determined using the StepOnePlus real-time PCR system (Applied Biosystems)
300 and calculated using the ΔΔCt method using GraphPad Prism. Gene expression was first
301 normalized using the housekeeping GAPDH gene in each sample, then the relative fold change
302 relative to experimental control. High Throughput 3' Digital Gene Expression (3'DGE) RNAseq
303 was performed on the isolated RNA using NovaSeq flowcells at the BioMicroCenter (MIT) and
304 processed using the BMC/BCC 1.8 pipeline (cocultures n=7; ESC monocultures, n=6).
305
306 ***2.11. Secreted protein measurement by ELISA and Luminex***
307 Spent media was stored at −80°C until analyzed by ELISA for prolactin (R&D Systems).
308 Protocols provided by the manufacturer were adapted to allow ELISAs to be performed in a

309 384-well plate (ThermoFisher) to minimize medium (sample) volume needed.[25] Multiplexed
310 Luminex assays were performed to measure cytokines in 48- or 72-hour undiluted conditioned
311 medium throughout the co-culture period using the magnetic Human Luminex XL Cytokine 45-
312 PLEX pre-mixed kit (R&D systems). Protocols provided by the manufacturer were adapted to
313 allow the assay to be performed in a 384-well plate to avoid introducing batch variability. Ten-
314 point standard curves with culture medium and assay buffer blanks were included for
315 quantification. Conversion from mean fluorescence intensity (MFI) values to absolute
316 concentration was performed by interpolating 5-parameter logistical fits of standard curves for
317 each analyte. Following the same downstream analysis protocol, secreted matrix
318 metalloproteinases (MMP) concentrations were measured using the magnetic Human MMP
319 Magnetic Luminex Performance Assay (R&D Systems). This assay required dilutions of cell
320 culture supernatants in fresh culture medium at either 2x or 200x to detect the reported analytes
321 within a quantifiable range.
322
323 ***2.12. Immunostaining and image analysis***
324 Hydrogel samples were fixed in 4% paraformaldehyde (Electron Microscopy Sciences) for 30
325 mins, permeabilized in 0.2% TritonX-100 in PBS (Sigma) for at least 30 mins at room
326 temperature, and then blocked overnight with blocking buffer (1% BSA (Sigma), 5% normal
327 donkey serum (Electron Microscopy Sciences) in PBS) at 4°C. Hydrogels were incubated with
328 primary antibodies overnight while rocking at 4°C, rinsed with blocking buffer 3 times (5 min
329 each while rocking at RT), and treated with secondary-conjugated antibodies overnight while
330 rocking at 4°C. Specific antibodies can be found in the supplementary table of reagents. Images
331 were captured using a ZEISS confocal Laser Scanning Microscope (LSM 880) or a Keyence
332 BZ-X800 Fluorescence Microscope. Image analysis was performed using Fiji open software and
333 3D image processing was performed using Imaris (Bitmap) software (9.6.0).
334
335 ***2.13. Endometrial ECM proteomics***
336 Endometrial ECM processing for proteomics, proteomics data collection, processing and
337 analysis is described elsewhere.[43] Briefly, fresh endometrial biopsies were collected and
338 processed using 50 µl of RapiGest (Waters Corporation) reconstituted in 50 mM NH_4HCO_3 at a
339 concentration of 2mg/ml to digest the endometrial biopsy sample for 24 hours at 37˚C. Next,
340 urea (ThermoFisher) and dithiothreitol (ThermoFisher) were added to the sample to bring the
341 mixture of a final concentration of 4 mM and 5 mM, respectively. Finally, iodoacetamide
342 (MilliporeSigma) was added to the sample, for a final concentration of 15 mM and kept in the

343 dark, at 37˚C, for 30 minutes. Samples were frozen at -80˚C until all patient samples had been
344 collected and processed. Samples were lyophilized overnight and then reconstituted in
345 NH_4HCO_3. Samples were digested with Trypsin Gold, mass spectrometry grade (Promega),
346 using a ratio of 1 µg trypsin to 50 µg sample protein as quantified using a Pierce BCA Protein
347 Assay Kit (ThermoFisher). Samples were digested overnight at room temperature using a rotor
348 for mixing and then placed in a speed vacuum to reduce sample volume. Dried down digested
349 peptide samples were labeled with TMT10plex kit (Pierce). After labeling, the samples were
350 mixed and purified with peptide desalting spin columns (Pierce). 1/5 of the sample was used for
351 one LC/MS/MS analysis (Thermo Exploris480 mass spectrometer). The dried peptide mix was
352 reconstituted in a solution of 2% formic acid (FA) for MS analysis. Peptides were loaded with the
353 autosampler directly onto a 50cm EASY-Spray C18 column (Thermo Scientific). All MS/MS
354 samples were analyzed using Sequest (Thermo Fisher Scientific; version IseNode in Proteome
355 Discoverer 2.3.0.523). Sequest was set up to search uniprot_human_reviewed_032120.fasta
356 (version March 21, 2020) assuming the digestion enzyme trypsin. Scaffold Q+ (version
357 Scaffold_5.0.1, Proteome Software Inc.) was used to quantitate Label Based Quantitation
358 peptide and protein identifications. Peptide identifications were accepted if they could be
359 established at greater than 10.0% probability to achieve an FDR less than 1.0% by the
360 Percolator posterior error probability calculation.[44] Normalization was performed iteratively
361 (across samples and spectra) on intensities, as described in Statistical Analysis of Relative
362 Labeled Mass Spectrometry Data from Complex Samples Using ANOVA.[45] Medians were used
363 for averaging. The protein list was then compared to the curated human matrisome
364 (http://matrisome.org/) list to look for ECM proteins. Samples were normalized using a mixed
365 aliquot of all patient samples that was analyzed in each LC/MS-MS run. Overlapping ECM
366 proteins found in all 3 LC/MS-MS runs were identified and the Limma package[46] in R was used
367 to remove batch to batch effects.
368

369 ***2.14. Endometrial tissue single cell RNA sequencing (scRNAseq)***

370 scRNAseq data collection, processing and analysis as described elsewhere (in preparation)[43].
371 Data was downloaded and Seurat (V3) was used to create dot plots and violin plots of specific
372 genes of interest on scaled data.
373

374 ***2.15. Bulk RNAseq analysis of in vitro co-cultures***

375 Aligned RNAseq transcript expected counts were analyzed in R (version 4.0.0) where data was
376 modeled using the edgeR package (version 3.34.0).[47,48] Counts were normalized by library size

377 and filtered to exclude genes with less than 20 transcripts across all samples. Principal
378 component analysis was performed using data batch-corrected by donor via the ComBat-seq
379 method of the sva package (version 3.13) in R, and each gene was scaled to have unit variance
380 before modeling.[49] Differential gene expression was calculated by modeling transcript data in a
381 quasi-likelihood negative binomial generalized log-linear model using the edgeR function
382 "glmQLFit". The use of a generalized log-linear model allowed for differences between hormone
383 treatment groups to be compared while accounting for inter-donor variability. Genes were
384 ranked by fold change in expression between hormone treatment groups to produce a ranked
385 list of genes for gene set enrichment analysis (GSEA)
386 (http://www.broadinstitute.org/gsea/index.jsp). Gene ontology (GO) term analysis was
387 performed on ranked gene lists of genes with pvalues <= 0.05. No adjustment was performed at
388 this step due to the low sample number, high variability, and intent to use the RNA sequencing
389 as a hypothesis generation step. The R package topGO (version 2.44.0) was used for GO term
390 identification and the package clusterProfiler (version 4.0.2) was used for visualizations. A
391 curated list of menstrual related genes was assembled from existing literature.[50,51] A heatmap of
392 $\log_2$ transformed data was created using the R package pheatmap (https://CRAN.R-
393 project.org/package=pheatmap; version 1.0.12) with the "complete" clustering method. Analysis
394 was performed on 7 co-culture experiments comprised of 5 donors, 2 independent technical
395 replicates and results were compared between experiments that were maintained in nEEO
396 media (N=2) or traditional EEO media (N=5).
397
398 ***2.16. Statistical analysis***
399 Data are expressed as average ± standard error of the mean (SEM). Statistical analysis was
400 performed using GraphPad Prism 8. Unpaired t-tests assuming unequal variances and two-way
401 ANOVAs with appropriate post-tests were performed. Holm-Sidak's multiple comparison of the
402 mean or two-tailed Mann- Whitney tests when comparing two groups. qPCR data was analyzed
403 using multiple t-tests. Statistical significance was defined as * $p < 0.05$, ** $p < 0.01$, *** $p <$
404 0.0001, and ****$P < 0.0001$.
405
406

407 **3. Results**

408

409 ***3.1 Design of a fully synthetic ECM guided by multi-omic evaluation of the human***
410 ***endometrium***

411 The ECM composition of the endometrium, along with cell-matrix receptor expression, are
412 regulated by sex steroids throughout the menstrual cycle,[52,53] giving rise to dramatic shifts in
413 tissue structure and morphology (Fig 1A). The overarching design goal for our synthetic ECM is
414 to define a minimal set of biophysical and biomolecular cues required to support the dynamic
415 phenotypic functions of heterogenous endometrial cell populations, over weeks of culture.

416 As a first step, we performed a targeted proteomic analysis (LC-MS/MS, N=11) of the
417 endometrial ECM-associated proteins (matrisome) across the menstrual cycle to benchmark the
418 ECM composition in the native tissue (Fig 1B). Consistent with immunohistochemical reports[54–
419 56], FN abundance was greater in the proliferative phase, while fibrillin, collagen and laminin
420 proteins increased during the secretory phase, corresponding to the differentiation of stromal
421 fibroblasts, epithelial gland maturation, and vascular remodeling in response to progesterone
422 (Fig 1B).

423 Our initial studies demonstrating the establishment of endometrial organoids in a synthetic
424 ECM[26] were guided in part by published histologic analysis of endometrial integrin expression
425 patterns from a subset of the 24 known integrins.[37,56–62] We sought additional insights into cell
426 population-specific integrin expression by probing a single cell RNA-sequencing dataset[43]
427 (scRNAseq, N=6; Fig 1C; Fig S1) to profile the integrin expression across the endometrial
428 proliferative or secretory phase epithelia and stroma in addition to the immune and vascular
429 cellular compartments. Across all cells in the data set, transcripts for all eighteen α chains and
430 all eight β chains, except integrin β3, were detected (data not shown). Integrin β3, a contested
431 marker of fertility that appears in the secretory phase[63–65], was also absent in another
432 endometrial scRNAseq data set.[66] Consistent with the immunohistochemistry literature[58], αV
433 was robustly expressed by epithelia and stroma mostly during the proliferative phase. Its
434 primary binding partner β5 was primarily expressed by the stroma across the cycle (Fig S1A),
435 while β6 was sparse except in proliferative phase epithelia (Fig S1A). Unexpectedly, integrin β8,
436 an additional αV partner that has not previously been characterized via immunohistochemistry
437 in the endometrium, was robustly expressed in several epithelial and some stromal
438 subpopulations (Fig 1C; Fig S1A). Also consistent with the immunohistochemistry data[56,59–61,67]
439 integrin β1 was robustly expressed by both epithelia and stroma across the cycle. Expression of

440 the collagen-binding α1 dimer (at lower levels, especially in proliferative epithelia) along with
441 strong expression of α2 in the epithelia was also observed, while the stroma primarily expressed
442 α5 (Fig 1C, Fig S1B). Finally, laminin-binding α6 and its heterodimer β1 was robustly expressed
443 in all epithelia, while expression in the stroma was higher in the proliferative phase (Fig S1). We
444 investigated the expression of a subset of these integrins in cultured endometrial cells via qPCR
445 confirming comparable expression of β1, α1, α2, α8 and αv in both stromal and epithelial cells,
446 and significantly greater expression of α5 and α8 in stromal cells (Fig S1C).
447 The minimal synthetic ECM must provide integrin-engaging adhesions cues needed by the
448 cells to support viability immediately post-encapsulation upon dissociation from tissue or a prior
449 culture state[68,69]. We thus include the peptide *GFOGER*, recognized by α1β1 (expressed on
450 stroma and epithelia) and α2β1 integrin heterodimers (expressed on epithelia),[70–72,73] together
451 with the fibronectin-derived *PHSRN-K-RGD* peptide [4,26] as an RGD ligand for αVβ1 and α5β1
452 (Fig 1D). This ligand incorporates the PHSRN synergy site recognized by α5β1 heterodimer
453 primarily expressed by the stroma and, to a lesser extent, by the secretory epithelium (Fig 1C).
454 As cells remodel the local microenvironment, proteolytically degrading the synthetic ECM,
455 they deposit cell-specific ECM, creating a dominant source of adhesion cues for a broad
456 spectrum of additional adhesion receptors as the culture progresses. To sequester this cell-
457 produced ECM and enhance its interactions with the synthetic ECM, we incorporated peptides
458 that bind to basement membrane components produced by epithelia (and some decidual
459 fibroblasts) and to fibronectin produced by stromal cells, as previously described.[25,26,31] This
460 strategy obviates the need to include laminin-derived peptides.[25,26,31]
461 To synthesize the synthetic ECM, we first functionalized an 8-arm poly(ethylene glycol)
462 (PEG)-based hydrogel with a combination of *GFOGER* and *PHSRN-K-RGD* ("*MIX*") in defined
463 ratios (see below), then crosslinked this macromer solution, in the presence of cells, with a
464 protease-degradable crosslinking peptide ("*CL-LW*") to enable cell-dependent matrix
465 remodeling, migration and proliferation during hormone-driven morphogenesis.[25,35,74] Using this
466 basic framework, individual synthetic ECM parameters (e.g., matrix stiffness) were
467 systematically and independently varied to mimic aspects of healthy and disease states (Fig
468 1D). Altogether, a tissue-inspired approach was implemented to design a synthetic matrix that
469 would initiate and maintain the culture of EEOs and ESC in a controlled environment that
470 mimics the molecular and biophysical properties of the endometrial ECM.
471

472 ***3.2 Synthetic ECM supports 3D co-culture of primary human endometrial stromal and***
473 ***epithelial cells***
474
475 *3.2.1. A semi-empirical screen of synthetic ECM properties yields a cue-response phenotypic*
476 *landscape for endometrial epithelial organoids.*
477 We previously demonstrated that a particular formulation of synthetic ECM designed for
478 enteric organoids also supported endometrial epithelial organoids[26]; however, the impact of the
479 biophysical properties and peptide composition on organoid phenotype and function was largely
480 unexplored. These first-generation hydrogels[26] incorporated only one adhesion ligand (i.e.,
481 *GFOGER*) and were substantially stiffer (~2000 Pa, corresponding to 5wt% PEG gels) than
482 Matrigel (~150-443 Pa)[20,75] or the native endometrial tissue (~250 Pa)[76]. Thus, to better
483 understand EEO generation in synthetic matrices, we probed the biophysical parameters that
484 more closely mimicked native endometrial stiffness and additionally interrogated the
485 consequences of integrin ligand composition. We first generated a tissue bank of EEOs from 8
486 endometrial donors, with and without endometriotic disorders (Table 1; Fig S2A) and defined a
487 panel of gels with varying elastic moduli, ranging from "soft" gels (3wt% PEG, ~ 300 Pa)
488 comparable to native stiffness of the endometrium, to the "stiffest" gels (7wt% PEG, ~6,000 Pa;
489 Fig 2A). To test these formulations, we dissociated organoids to single cells, passaged them
490 into synthetic matrix or Matrigel, and followed the emergence into single cell-derived
491 endometrial epithelial organoids ("scEEO", Fig S2B). In agreement with our previous work[26],
492 employing synthetic hydrogels functionalized with *GFOGER* was sufficient to support the growth
493 of scEEOs, even in a relatively stiff (5wt% PEG) environment. However, scEEOs generated in
494 the stiffer gels developed a crenelated morphology (Fig 2B; Fig S4) compared to those cultured
495 in softer conditions (3wt% PEG), and this was consistent across all donors regardless of the
496 donor's disease state (data not shown).
497 Anticipating the integration of α5β1-expressing stromal cells, we then evaluated the influence
498 of an additional integrin ligand on scEEO growth behavior and morphologies. We compared
499 ECM formulations incorporating nominal concentrations of *GFOGER* (3mM), *PHSRN-K-RGD*
500 (3mM), or a *MIX* of both peptide (1.5 mM each) in the soft (~300 Pa, 3wt% PEG) gel regime.
501 Biomechanical properties were not significantly affected by differences in integrin ligand
502 composition (data not shown). As expected, *GFOGER* was necessary to generate scEEOs in
503 synthetic matrices (Fig 2C; Fig S3), presumably through engagement of α1β1 and α2β1, and
504 although *PHSRN-K-RGD* conferred minimal scEEO generation alone, incorporation of both
505 adhesion ligands in the *MIX* formulation robustly promoted the growth of the scEEO despite the

506 lower (1.5 mM vs 3 mM) concentration of GFOGER in the *MIX* (1.5 mM *GFOGER* + 1.5 mM
507 *PHSRN-K-RGD*) formulation. When visualized by brightfield imaging on sequential days after
508 seeding single cells, organoids appeared to emerge more slowly in PEG matrices (soft, 3wt%)
509 than in Matrigel, yet they retained similar morphologies and diameters by day 9 of culture (Fig
510 2D) suggesting that the 3wt% gels function with comparable efficacy to Matrigel.
511 Having confirmed the requirement for *GFOGER*, and comparable scEEO emergence in both
512 *GFOGER*-only and *MIX* gels, we next compared how matrix stiffnesses impacted scEEO
513 emergence by varying the PEG polymer content from 3wt% (~300 Pa) to 7wt% (~6 kPa) to
514 mimic physiologic[76] and pathologic[77] uterine regimes, respectively (Fig 2E-F). The efficiency of
515 scEEO formation, as assessed by the number of organoids at day 14 relative to Matrigel, was
516 slightly inversely correlated with matrix stiffness (Fig 2E). Moreover, organoid diameter
517 distributions in stiffer matrices, where organoids were sparser, skewed slightly higher in the
518 5wt% and 7wt% gels compared to softer 3wt% matrices (Fig 2F). Consistently, the organoids
519 cultured in stiffer matrices (5wt% and 7wt%) manifested the meandering, crenelated
520 morphology described above, but not in softer PEG matrices or Matrigel (Fig S4). These results
521 suggest that EEO clonal establishment is robust across a range of biophysical properties (Fig
522 2E-F) and provide a preliminary indication that tissue stiffness influences epithelial morphology
523 and behaviors.
524 Based on these results, we focused further investigations using the more physiologically
525 relevant 3wt%-*MIX* gels to characterize scEEO architecture, hormone response and cellular
526 heterogeneity in the synthetic ECM. PEG-derived scEEOs exhibited proper polarity based on
527 basolateral laminin (LMN) deposition and apical F-actin accumulation, comparable to those
528 generated in Matrigel (Fig 2G). Moreover, scEEOs generated in synthetic matrices retained their
529 epithelial origin and architecture as assessed by EpCAM and F-actin staining (Fig S5A-B), were
530 mitotically active (Fig S5C), and exhibited appropriate response to sex steroids as demonstrated
531 by immunohistochemical staining of progesterone receptors (PGR) (Fig 2H) and the
532 downregulation of PGR transcript, but not ESR, in response to progestin treatment (Fig 2I). To
533 confirm scEEO maturation, live-imaging and immunostaining revealed distinct populations of
534 motile ciliated and secretory epithelial cells (Fig S5D, Video 1). These results were consistent
535 across several tissue donors (N=8). Altogether, these results justified the use of soft (3wt%)
536 PEG hydrogels, functionalized with a dual presentation of *GFOGER* and *PHSRN-K-RGD* (*MIX*),
537 as a functional synthetic ECM to generate and maintain long-term cultures of endometrial
538 organoids (Fig 1D).
539

540 *3.2.2. Establishment and characterization of ESC 3D cultures in synthetic ECM*

541 Our results examining organoids in synthetic matrices demonstrated that both the biophysical
542 and the molecular parameter space of the hydrogels are important to promote adequate scEEO
543 growth and function; therefore, we set out to evaluate, in parallel, how adhesive cues and matrix
544 stiffness influenced ESC behavior in 3D (Fig 3A). Embedded ESCs cultured in the gels were
545 viable in all conditions tested (*GFOGER*, *PHSRN-K-RGD*, or *MIX* for the 3-7% PEG) and
546 maintained comparable cell numbers across all conditions (data not shown). However, ESCs
547 adopted a more characteristic stellate morphology in softer (3wt%) hydrogel microenvironments
548 compared to the stiffer (5wt%) gels which constrained fibroblast spreading and outgrowth (Fig
549 3B; 7% not shown). Furthermore, in support of previous studies[25], hydrogels containing
550 *PHSRN-K-RGD* further provided a modest increase in stromal dispersion and spreading, as
551 assessed by the fluorescence projected area covered on day 7 of culture, compared to matrices
552 containing *GFOGER* alone where cells retained a more clumped distribution (Fig 3C).

553 Although the ESCs can enzymatically remodel the synthetic matrices due to the
554 incorporation of the MMP cleavable crosslinker, PEG gels remained intact at the 15-day time
555 point, whereas cultures in Matrigel or collagen I gels have shrunken and at least partly
556 disintegrated by this time point (Fig 3D). This ability to maintain long-term cultures enabled us to
557 assess stromal function in the gels by maintaining the 3D cultures under sex hormone
558 stimulation throughout the 15-day experiment. In response to treatment with E_2 (E), a synthetic
559 progestin (E_2 + MPA, "PE"), or a PE hormone withdrawal (72 hrs, 'W'), subsets of ESCs
560 underwent decidualization, a differentiation process necessary for the establishment of
561 pregnancy, characterized by the secretion of pro-gestational protein prolactin (PRL) and
562 morphological changes toward an epithelial-like decidual cell.[42,51,78] Although increased matrix
563 stiffness curtailed ESC elongation in the E-containing medium before decidualization, ESC
564 developed characteristic rounded epithelioid morphologies in response to progestin in the *MIX*
565 gels, in both standard ESC culture media as well as EEO media (Fig 3E). Detection of PRL
566 secretion in the spent media confirmed that ESC embedded in 3D gel underwent robust
567 decidualization in all matrix stiffnesses response to progestin treatment (Fig 3F), suggesting that
568 stiffness is not a strong influence on this metric of stromal hormone sensitivity.

569 We next investigated the effects of exogenous treatment with IL-1β (1 ng/mL), a pro-
570 inflammatory cytokine associated in reproductive disorders[79], on ESC phenotype in the
571 synthetic gels. Compared to control groups, which exhibited robust proliferation at day 15 in the
572 3wt% *MIX* hydrogel in both E and PE media, as 50-60% of cells incorporated EdU over a 24-
573 hour incubation period (Fig 3G-H), IL-1β dramatically suppressed ESC mitotic activity resulting

574 in ~5% of cells incorporating EdU (Fig 3G) and induced an increase in apoptosis (Fig 3I).
575 Furthermore, by day 15, treatment with IL-1β also dramatically suppressed PRL production
576 even in the presence of the progestin MPA (Fig 3J). Brightfield and immunofluorescent
577 examination of stromal morphology in response to the inflammatory cue revealed a drastic
578 change toward an elongated morphology, characterized by a thin architecture (Fig S6A-B) and
579 decreased cell surface area (Fig S6C). This change was attributed to an apparent increase in
580 ECM remodeling capacity characterized by increased cellular motility (Video 3). These results
581 suggest that despite a reduction of mitotic activity, IL-1β induces a more activated ESC
582 phenotype in 3D. In line with this result, morphological assessment revealed that ESC cultured
583 in Matrigel also developed the phenotype akin to those exogenously treated with IL-1β (Fig 3D),
584 highlighting the limitations conferred by Matrigel to study stromal behavior[27]. Altogether, these
585 results demonstrate that the relatively soft, dual integrin ligand (3wt% *MIX*) synthetic matrix
586 formulation is suitable as a "one size fits all" scaffold for culturing both stromal cells and
587 epithelial organoids.
588
589 *3.2.3. Engineered synthetic matrices support the stable co-culture of EEO and ESC, capturing*
590 *the temporal physiologic processes of the human menstrual cycle*
591 In the endometrium, both stromal and epithelial cells express hormone receptors for
592 estrogen and progesterone, yet proper tissue-level function is mediated by the crosstalk
593 between these cell types.[80–83] Parsing this crosstalk *in vitro* using Matrigel - which contains
594 numerous exogenous growth factors, rapidly degrades, and largely lacks the physiologic ECM
595 molecules for stromal cells – is arguably a fraught endeavor. Thus, we used the fully defined
596 synthetic matrices described to develop a co-culture model using defined cell ratios that were
597 shown to approximate those observed *in vivo* (Fig S7) to interrogate these dynamic
598 phenomena. Donor matched EEOs and ESCs populations (N=12) were co-cultured in the
599 synthetic ECM (3wt%-*MIX*) using a fully defined common media (see Methods) and maintained
600 for up to 15 days of culture (Fig 4A; Video 2,3). Immunostaining demonstrated the persistence
601 of morphologically well-defined stromal and epithelial populations (Fig 4B; Video 2). All cultures
602 were viable, with minimal cell death, throughout the length of the experiments as demonstrated
603 by live/dead staining (Fig S12) at day 15. Co-cultures were exposed to hormone stimulation
604 designed to mimic the proliferative (E_2, 'E'), secretory (E_2 + MPA, 'PE'), or menstrual (72 hr PE
605 withdrawal + RU-486, 'W') phases of the idealized human menstrual cycle (Fig 4C-D).
606 To determine whether the PEG-based co-culture model could phenocopy canonical
607 molecular pathways involved in the human menstrual cycle, we characterized the co-cultures (N

608 = 5 donors) by both transcriptomic and functional analysis after hormonal treatment. First, we
609 implemented bulk RNA sequencing (n=7) and demonstrated that after 15 days, co-cultures were
610 transcriptionally distinct from either ESC or EEO monocultures (Fig S8B, Fig S19). Further
611 analysis using a generalized linear model compared gene expression between ESC
612 monocultures and co-cultures using Benjamini-Hochberg (BH) multiple hypothesis test
613 correcting[84], resulted in 7,821 genes to be differentially expressed at an adjusted p-value
614 threshold of 1×10^{-5} (Fig S8C). These findings are suggestive of a crosstalk between these
615 stromal and epithelial populations when cultured together.
616 Next, we analyzed the response of co-cultures with respect to hormonal signaling
617 pathways. Further transcriptomic analysis of the co-cultures by hierarchical clustering
618 demonstrated that the expression of endometrium-associated genes segregated samples by
619 hormonal treatment rather than donor variability (N=2 donors), and adequately reproduced gene
620 expression profiles associated with their respective menstrual cycle phases (Fig S9A). To
621 identify the molecular functions, biological processes, and pathways differentially regulated by
622 the hormone treatments, we performed Gene Ontology (GO) analysis and detected key
623 reproductive biological processes associated with progesterone signaling to be significantly
624 ($p>0.05$) enriched in secretory and menses groups, including ECM composition and receptor
625 signaling activity (Fig 4E). Gene network visualizations of these pathways confirmed that, in
626 response to hormone treatment, the co-cultures reproduced progesterone-induced expression
627 of specific secretory phase associated genes including PRL, PAEP, and ECM-associated genes
628 and downregulation of CPM, MMP9, and cytokine-mediated inflammatory genes (Fig S9B).
629 Finally, gene set enrichment analysis (GSEA) further confirmed recapitulation of canonical
630 menstruation-associated hallmarks (Fig S10D), including significant upregulation of
631 senescence, inflammatory[80], and hypoxia[85] in the withdrawal treatment group compared to E or
632 PE (Fig 4F). To expand on these transcriptomic findings, we also observed expression of matrix
633 metalloproteinases (MMPs), including those primarily produced by either the stromal (e.g.,
634 MMP-2) or epithelial populations (e.g., MMP-7, MMP-26).[10,86] To corroborate these
635 transcriptomic findings, we also measured temporal changes in matrix metalloproteinases
636 (MMPs) from the spent media (Fig S14C). Together, we co-cultures recapitulated similar
637 temporal expression trends that are observed *in vivo*[87,88], specifically a reduced MMP-1, -3 and -
638 10 expression in the secretory phase compared to proliferative group and reduced MMP-2
639 compared to the menses group (Fig S10C).
640 Finally, we experimentally validated the co-culture model using functional assays to assess
641 the morphologic and biochemical changes observed across the human menstrual cycle. First,

642 we examined whether the model captured morphologic features of secretory endometrial glands
643 in response to hormonal stimulation observed *in vivo* (Fig 5A). Progestin treatment caused
644 changes in EEO morphology characterized by thickening of the pseudo-stratified columnar
645 epithelial layer and increased epithelial invaginations (Fig 5B, Fig S10A). Moreover, epithelial
646 secretory function was demonstrated by positive staining of progestogen-associated
647 endometrial protein (PAEP), a marker of the secretory epithelium, in the lumens of the
648 organoids treated with progestin (Fig 5C; Fig S10B). Similarly, a robust induction of stromal
649 decidualization in response to progestin also occurred in the co-cultures by day 15 of the
650 experiment resulting in increased secretion of PRL in the secretory groups and reduced in the
651 menses group (Fig 5D). Moreover, the characteristic negative regulation of PGR during the
652 secretory phase compared to the proliferative phase observed *in vivo*[89,90] was demonstrated via
653 immunostaining in both epithelial and stromal populations *in vitro* (Fig 5E). In accordance with
654 literature observations[6], the temporal analysis across the 15 days showed that co-cultures
655 maintained in baseline E2 conditions showed no significant increase in PRL (Fig 5F), but co-
656 cultures treated with the progestin MPA showed a significant increase in PRL production
657 starting 9 days after MPA treatment initiation (Fig 5F). Finally, we also observed a significant
658 ($p=0.031$, N=3) doubling of apoptosis (Fig 5G-H; Fig S11) in epithelial glands of the co-cultures
659 in the menses groups (3.06 $Casp^+/cm^2$) compared to the secretory groups (1.37 $Casp^+/cm^2$)
660 mimicking the increased cell death observed during the induction of menstrual phase in vivo.[91,92]
661 Altogether, these results demonstrate the establishment of a co-culture model of the
662 endometrium can recapitulate *in vitro* several of the hormone-induced phenotypic, morphologic,
663 and biochemical changes associated with the idealized human menstrual cycle and could be
664 used to investigate on reproductive function in mechanistic fashion.
665
666 *3.2.4. Progesterone action is disrupted by IL-1β treatment in the co-culture model*
667 The suppression of stromal cell response to progestin in the presence of IL-1β (Figs 3H,J)
668 motivated us to analyze the molecular and phenotypic responses of epithelia and co-cultured
669 stromal and epithelial cells to IL-1β, anticipating outcomes in the latter case would likely be
670 influenced by stromal-epithelial cross talk. Separate proliferative, secretory, and menses
671 treatment groups were co-stimulated with IL-1β (1 ng/mL) throughout the 15-day experiment
672 (Fig 4D). First, in accord to the results described above (Fig S6), the stromal population in co-
673 cultures also developed an elongated (inflamed) morphology (Fig S15). Furthermore, co-
674 cultures exposed to the inflammatory stimulant IL-*1*β showed suppression of a canonical
675 decidualization response, production of PRL after extended (week or more) exposure to a

676 progestin, as in E (Fig 5F). Whereas the control co-cultures showed a canonical increase in
677 production of PRL following a week of progestin exposure and continued increase through the
678 15 days of treatment (Fig 5F), PRL production in control co-cultures treated with IL-1β showed
679 no difference in PRL production in the presence or absence of progestin; both E and E+P co-
680 cultures treated with IL-1β showed an unexpected spike in PRL production in the immediate 3
681 days after stimulation with the inflammatory cue followed by a fall to negligible levels for the
682 remainder of the 15 days (Fig. 5F). Analysis of the inflamed (IL-1β treated) co-cultures by bulk
683 transcriptomic (Fig S13) and multiplex immunoassay (Fig S14) analysis confirmed the
684 decreased PRL expression observed at the protein level (Fig S13B). Gene expression analysis
685 in a generalized linear model using 8,423 genes expressed across all samples comparing
686 controls to IL-1β stimulated cocultures (Fig S13A) revealed an expected global up-regulation of
687 several additional pro-inflammatory cytokines and chemokines (e.g., IL6, TNF-α, CCL2, CCL8,
688 CCL5) and down-regulation of anti-inflammatory cytokines (e.g., IL10) in the IL-1β -treated
689 groups (Fig S13B). Hallmark pathway enrichment analysis of the unstimulated and IL-1β-
690 stimulated co-cultures detected disruptions of progesterone-regulated pathways including the
691 downregulation of ECM structural constituent, and upregulation of inflammatory receptor-ligand
692 signaling processes (Fig S13C). Immunostaining revealed that co-cultures with IL-1β, compared
693 to the untreated controls, further increased apoptosis in the transition from the secretory to the
694 menses phase (Fig 5H; Fig S11), an observation that was corroborated by a separate assay of
695 cell death (Fig S12). These findings show that IL-1β can disrupt progesterone actions. We
696 confirmed this via immunostaining for PGR expression in the co-cultures which showed reduced
697 PGR signal, even in the E-containing media, (Fig 6A) in both the epithelial and stromal
698 populations.
699 Lastly, stimulating the co-cultures with IL-1β caused a significant flattening of epithelial
700 morphology causing a shift from the pseudo-columnar architecture in the controls toward a
701 squamous cell structure with thin apical F-actin staining (Fig 6B). Whereas progestin treatment
702 significantly increased cell height in the control co-cultures, as characterized by the distance
703 from apical to basolateral side (E vs PE; $p=0.0098$), in the IL-1β -treated groups, epithelial cells
704 were thinner than in controls (PE vs PE+IL-1β; $p < 0.0001$) and were relatively unaffected by
705 progestin (Fig 6C). This flattening phenomenon closely mimics the de-differentiation events
706 observed in the wound repair cell response of the intestine.[93] The change in morphology of the
707 epithelial cells was accompanied by a slight, but non-significant ($p=0.127$), increase in spacing
708 between nuclei compared to the round nuclei in the controls at the single cell level (Fig 6B, Fig
709 S16A), suggesting the flattened cell in the IL-1β treated groups have a slightly increase in

710 projected cell area compared to the controls to compensate for the reduction in cell height while
711 keeping similar volume. An alternate metric of projected cell area, the density of nuclei counted
712 per area of organoid monolayer surface, was comparable in control and IL-1β- treated co-
713 cultures (Fig S16B). Further analysis of the morphometric changes cell volume is a topic for a
714 future investigation. Altogether, these results highlight the extent by which IL-1β can promote
715 the overexpression of additional pro-inflammatory cytokines associated with reproductive
716 diseases[94–96] and can potentiate progesterone resistance, a phenomenon that is a characteristic
717 feature of endometriotic disease *in vivo*[97,98].
718
719 ***3.3 IL-1β treatment disrupts epithelial proliferation via a stromal-dominant***
720 ***communication***
721 Chronic inflammation of ectopic lesions is a characteristic feature of endometriosis; wherein
722 endometrial epithelial and stromal cells are found growing outside the uterus.[99] We thus next
723 assessed whether inflammation altered epithelial proliferation in ways that may illuminate
724 mechanisms of disease. Tissue-recombinant murine models have previously demonstrated that
725 estrogen and progesterone mediate epithelial mitogenic processes indirectly through signals
726 from the hormone-responsive stromal fibroblast,[83,100,101] therefore hypothesized that IL-1β may
727 exert its effect via similar mechanisms. To test this, we measured the effects of IL-1β treatment
728 on epithelial growth, in epithelial monocultures and in co-cultures (Fig 6D; N=4 donors, matched
729 cultures), using both morphological analysis of organoid diameters and measuring DNA
730 synthesis.
731 First, we measured changes in organoid size (outer diameter) across the 15 days of culture
732 as a proxy for growth rates (Fig S17A). As observed with endometrial stromal cells in
733 monoculture (Fig 3G-H), IL-1β treatment significantly (PE vs PE+IL-1β; $p=0.0121$) suppressed
734 the growth of the epithelia in monoculture, compared to controls, using the metric of organoid
735 diameter (Fig S17A). Unexpectedly, in co-culture with stroma, IL-1β treatment caused an
736 observable increase in epithelial organoid diameter compared to untreated controls (Fig 6E).
737 Quantification of the organoid diameter across the 15 days of culture demonstrated that IL-1β
738 stimulation positively impacts scEEO diameter growth in the co-cultures, but not in the
739 monocultures (Coculture vs monoculture; $p=0.0026$) resulting in a mean fold change in organoid
740 diameter of 7.3 and 3.9-fold in the co-cultures and monocultures, respectively (Fig 6F).
741 As scEEO diameter is only a proxy for changes in cell number, the mitotic activity of these
742 cultures at day 15 was examined by measuring EdU incorporation by the organoids after 24
743 hours of incubation (Fig 6G). In organoid monocultures there was a non-significant ($p > 0.05$)

744 trend toward reduction of DNA synthesis in scEEOs upon treatment with IL-1β (E=1822;
745 PE=2333; E+IL-1β=1185; PE+IL-1β=1407 EdU^+/mm^2; N=3) and a surprising trend toward
746 increase in DNA synthesis in the presence of progestin compared to E-only conditions (Fig 6H).
747 In stark contrast, stimulation with IL-1β resulted in a greater than 3-fold increase (PE = 228;
748 PE+IL-1β = 978 EdU^+/mm^2; P= 0.0014; N=4) of scEEO DNA synthesis in cocultures compared
749 to controls (Fig 6I), consistent with the observed increase in organoid diameters in IL-1β treated
750 co-cultures (Fig 6E). Further, unlike monocultures, the proliferative index of scEEOs in co-
751 culture decreased in progestin-treated controls compared to E-only controls, as would be
752 expected in the transition from proliferative to secretory phase *in vivo*[102]. Unexpectedly, the
753 proliferative index of scEEOs in co-cultures treated with IL-1β showed the opposite trend to that
754 of monocultures when progestin was added– an increase in the proliferative index compared to
755 E-only cultures (Fig 6E). These phenotypic changes in epithelial mitotic activity mirror the
756 increased epithelial proliferative profiles observed in the eutopic and ectopic endometriotic
757 tissues in vivo.[103,104] Although the scEEO monocultures appeared to have a greater proliferative
758 index than the co-cultures in some groups, this difference could be attributed to the contribution
759 of the ESC in mediating hormone signaling, as shown in other models.[105]
760 Perhaps because of this increased growth rate, IL-1β stimulation in co-cultures resulted in
761 greater organoid collapse by day 15 and could also explain the ~1.5-fold (p=0.012) increase in
762 apoptosis (Casp-3^+ staining) observed in the epithelial (Fig 5G) populations that resulted in an
763 overall increase in cell death (ethidium homodimer staining, Fig S12). Altogether, these results
764 support a working model by which inflammatory signals and sex hormone signaling in the
765 endometrium are partially mediated indirectly via the stroma (Fig 6J).

766 **Discussion:**

767 The endometrium is a marvelous example of regenerative biology wherein sex hormones
768 mediate rapid growth and maturation of the tissue, accompanied by equally dynamic changes in
769 ECM-cell interactions that are both mechanically and molecularly linked to reproductive
770 function.[106] These remarkable regenerative properties also contribute to common debilitating
771 diseases like endometriosis, for which new therapies are desperately needed. Here, we
772 developed a new model for dissecting molecular and phenotypic consequences of endometrial
773 epithelial-stromal crosstalk in long term (15 day) cultures of patient-derived endometrial cells by
774 defining a completely synthetic extracellular matrix hydrogel that is tailored to both replace
775 Matrigel for organoid culture, and simultaneously to support stromal culture. We then used this
776 model to show how the hormone-dependent behaviors of the endometrial epithelium in co-
777 culture with stroma diverge from those in monoculture, observing for example that the pro-
778 inflammatory cue IL-1β appears to drive the endometrial co-cultures, but not monocultures, to a
779 state that phenocopies features of diseases like endometriosis.[95,99]

780 The synthetic ECM described here overcomes certain limitations of organoid technologies
781 and other co-culture approaches for parsing cell-cell communication in general, especially in the
782 endometrium. Natural matrices like Matrigel and collagen – which have been used either alone
783 for co-culture[27,28,42,107] or combined in creative ways[108,109] – include many extraneous signaling
784 molecules that may drown out the signals produced by the cells they support. This limitation is
785 underscored by the inability to design experiments that require longer term stable cultures, as is
786 the case for hormone signaling, or need specific ECM stiffness. The main constituent of this
787 synthetic ECM, PEG, is a blank slate known for its relative lack of interaction with proteins.
788 Thus, growth factors, cytokines, and other molecules produced by each cell type can freely
789 dominate the cell-cell communication networks. By design, the synthetic ECM comprises only a
790 minimal set of biological cues: two integrin ligands, two ECM-binding proteins, and a peptide
791 crosslinker, all produced by standard, well-defined chemical peptide synthesis methods. These
792 minimal cues, which were modified from a previous formulation used for organoids[26] and
793 monolayer cell line co-cultures[25], include ligands for a spectrum of integrins expressed
794 differentially by epithelial and stroma (see Results) and enable cell-mediated remodeling of the
795 microenvironment as well as the accumulation of cell-produced ECM. By demonstrating that this
796 synthetic matrix is sufficient to generate scEEOs from the original primary glands without the
797 need to first expand in Matrigel (Fig S18), we provide a hydrogel alternative to alleviate the
798 dependency on Matrigel. Because the synthetic matrix is relatively simple and is chemically
799 defined, it is straightforward to implement reproducibly for the culture of organoids and co-

800 cultures. Reproducibility within and between labs is highly desirable to analyze phenotypes of
801 patient-derived tissue models due to the inherent biological variability in the samples
802 themselves. Finally, although only an initial characterization is provided here, the synthetic ECM
803 arguably offers greater potential to mimic and study certain features of endometrial diseases
804 compared to ECM-free co-culture models[110,111], as its biophysical properties can be tuned
805 systematically to mimic the "soft" regimes of healthy endometrium or the "stiff" regimes of the
806 myometrium[112] or fibrotic tissue (Fig 2A).
807 Steroid hormone-driven stromal-epithelial crosstalk in the endometrium has been illustrated
808 in mouse models involving cell type-specific receptor knockouts in the eutopic endometria[89,113]
809 and recombinant implantation of tissue fragments in the renal capsule,[105,114] but crosstalk in
810 normal and diseased human co-cultures has been more challenging to parse due to the
811 disparate matrix environments preferred by each cell type[115,116], and the relative short-lived
812 nature of cultures in Matrigel or collagen. For example, work by Rawlings and co-workers
813 showed stromal-epithelial crosstalk enabled a simplified medium to support an elegant collagen
814 gel-embedded "assembloid" co-culture model that captured both normal and drug-skewed co-
815 evolution of the stromal population to subpopulations of decidual and acutely senescent
816 fibroblasts[42]. They thus defined a tantalizing model for analysis of embryo implantation if the
817 limitations of the culture longevity, which disintegrate before the entire sequence of implantation
818 steps is realized under some conditions, and the limited access organoid apical interface, can
819 be overcome[42]. Thus, the long-term capacity of co-cultures in our synthetic hydrogel may
820 provide one approach to extending the assembloid model if similar evolution of fibroblasts
821 populations can be demonstrated. In concordance with a different short term (7-day) co-culture
822 model, employing EEOs cultured in Matrigel in a Transwell membrane above a coverslip coated
823 with stroma[117], we observed the expected suppression of proliferation by E_2 and P4 compared
824 to E_2 in control co-cultures (Fig 6F and Fig S17). However, we are also able to observe more
825 pronounced effects at the two-week time point, especially in cultures treated with IL-1β (Fig 6F
826 and Fig S17) and provide evidence that the inflammatory cue IL-1β can also modulate epithelial
827 proliferation via the stroma (Fig 6J).
828 Indeed, the responses of co-cultures to inflammatory cues at extended time points are
829 the most striking findings in this study, as they may shed light on endometrial disorders closely
830 associated with pro-inflammatory cytokines such as TNF-α and IL-1β.[94] In co-cultures treated
831 with IL-1β, organoid diameter (Fig 6F) and epithelia mitotic activity (Fig 6I) are both increased,
832 even in the presence of MPA, compared to the E2 condition, whereas the canonical response to
833 progestin is a decrease in epithelial proliferation, as observed in the control co-cultures and in

834 monocultures. We speculate that this observation of an IL-1β-MPA synergy may have clinical
835 relevance for the observed failure of some endometriosis patients to respond to progestin
836 therapies. Similar to our observations about IL-1β inducing profound epithelial flattening along
837 with increased proliferation, in deep infiltrating endometriosis lesions, an "invasive front"
838 characterized by highly flattened epithelia with greater proliferative index than epithelia in a
839 more quiescent core has been described[118]. Furthermore, greater proliferation indices are
840 observed in the eutopic endometrium of endometriotic patients, compared to controls[102,104].
841 While more translational validation is warranted to confirm mechanistically similar behaviors, the
842 results are suggestive that the model may capture features that are important clinically.
843 Importantly, the timely and acute induction of inflammatory mediators are also well known to
844 be critical for maintaining normal reproductive physiology[79]. This may explain why a transient
845 (day 3) increase in PRL secretion was observed in the co-cultures in response to IL-1β as
846 acute-phase inflammatory insults that activate the nuclear factor–kappaB (NF-κB) system, a
847 master regulator of cell survival and proliferation in endometriotic disease[119], have been shown
848 to regulate PGR expression in vivo[79,89], and can enhance stromal decidualization and blastocyst
849 implantation[55,120] A limitation of this study is that most assays were performed at end point
850 measurements (day 15), future mechanistic studies that dissect the timing (acute vs chronic),
851 abundance (low vs high concentration), and synergism with sex hormones (estrogenic vs
852 progestin conditions) will be critical to fully understand the extent by which IL-1β can positively
853 promote physiologic (e.g., implantation) or induce pathologic processes (e.g., endometriosis,
854 infertility)[98,119], and ultimately will help identify therapeutic approaches for targeting the disease
855 while maintaining reproductive function (Fig 6J).
856 Finally, we are just beginning to explore how the properties of the synthetic ECM may
857 enable more complex tissue-level architectures than the relatively simple organoid-stroma
858 culture described herein. For example, we have observed that organoids close to the gel-liquid
859 interface sometimes merge with each other and erupt to form mature epithelial organoid-
860 monolayers structures that are more representative the glandular-luminal epithelial
861 compartment of a true endometrial mucosal barrier (Fig S21). We are now defining protocols
862 that foster efficient and reproducible fusion. A parallel effort to represent the heterogenous cell
863 populations of the endometrial microenvironment combines immune cells with stroma and
864 epithelia, as we have described for pancreatic tumors[31], with an eye toward addition of these
865 complex endometrial models to perfusable blood vessels maintained in microfluidic devices,
866 extending our initial findings that we can form microvascular networks in synthetic PEG
867 gels[121,122]. We speculate that the co-culture model described here can be productively extended

868 by the research community as a platform to mechanistically parse stromal-epithelial crosstalk in
869 the human endometrium.
870
871 **Acknowledgements:** We thank the Newton Wellesley Hospital staff for facilitating a tissue
872 collection program with MIT and the patients that donated their tissues for our research. We
873 thank Histology Facility at the Koch Institute at MIT for their assistance with histological
874 processing of tissues. We thank Profs. Kevin Osteen and Kaylon Bruner-Tran at Vanderbilt
875 University for their support. J.S.G. was supported by an Environmental Toxicology Training
876 Grant (NIH T32 ES007020) and from the Bill and Melinda Gates Foundation. Additional funding
877 was provided by The John and Karine Begg Foundation, the Manton Foundation, and NIH U01
878 (EB029132).
879
880 **Author Contributions:** J.S.G. and A.T.B. conceived the study, designed, performed, and
881 analyzed the experiments. J.S.G. wrote the manuscript. J.S.G isolated, cultured and maintained
882 primary cell populations with the help of C.I. and L.B. In Vitro culture data processing and
883 analysis was performed by J.S.G., A.T.B., and K.B. Hydrogel and tissue biobank was
884 maintained by V.H.G, and C.I. Ex Vivo analysis was performed by B.G. and L.B. for scRNAseq
885 and proteomics, respectively. All were involved in editing the manuscript. M.L., K.I., and J.S.G.
886 supervised tissue collection and processing. L.G.G. supervised project development and edited
887 the manuscript.
888
889 **Competing Interests statement:** L.G.G. and V.H.G. have a patent application pending related
890 to the hydrogel system. The rest of the authors have no competing interests.
891
892 **Data availability**. Source data are available upon request from the corresponding author.

893 **4. References:**

894

895 1. Aplin JD. Cellular Biochemistry of the Endometrium. In: *Biology of the Uterus*. Vol 20.
896 Karger Publishers; 1989:89-129. doi:10.1007/978-1-4684-5589-2_6
897 2. Aplin JD, Ruane PT. Embryo-epithelium interactions during implantation at a glance. *J Cell*
898 *Sci*. 2017;130(1):15-22. doi:10.1242/jcs.175943
899 3. Noyes R, Hertig A, Rock J. Dating the endometrial biopsy. *Obstet Gynecol ….* Published
900 online 1950.
901 4. Loy SLY and TS. Normal cycling Endometrium:Molecular, Cellular, and Histologic
902 Perspectives. In: *Endometriosis in Clinical Practice*. ; 2005:1-29.
903 5. Roy A, Matzuk MM. Reproductive tract function and dysfunction in women. *Nat Rev*
904 *Endocrinol*. 2011;7(9):517-525. doi:10.1038/nrendo.2011.79
905 6. Brosens JJ, Hayashi N, White JO. Progesterone receptor regulates decidual prolactin
906 expression in differentiating human endometrial stromal cells. *Endocrinology*.
907 1999;140(10):4809-4820. doi:10.1210/endo.140.10.7070
908 7. Kelleher AM, Demayo FJ, Spencer TE. Uterine Glands: Developmental Biology and
909 Functional Roles in Pregnancy. *Endocr Rev*. 2019;40(5):1424-1445. doi:10.1210/er.2018-
910 00281
911 8. Cameron IT, Fraser IS, Smith SK (Stephen K. *Clinical Disorders of the Endometrium and*
912 *Menstrual Cycle*. Oxford University Press; 1998.
913 9. Boretto M, Cox B, Noben M, et al. Development of organoids from mouse and human
914 endometrium showing endometrial epithelium physiology and long-term expandability.
915 *dev.biologists.org*. Published online 2017. doi:10.1242/dev.148478
916 10. Turco MY, Gardner L, Hughes J, et al. Long-term, hormone-responsive organoid cultures
917 of human endometrium in a chemically defined medium. *Nat Cell Biol*. 2017;19(5):568-577.
918 doi:10.1038/ncb3516
919 11. Clevers H. Modeling Development and Disease with Organoids. *Cell*. 2016;165(7):1586-
920 1597. doi:10.1016/j.cell.2016.05.082
921 12. Boretto M, Maenhoudt N, Luo X, et al. Patient-derived organoids from endometrial disease
922 capture clinical heterogeneity and are amenable to drug screening. *Nat Cell Biol*.
923 2019;21(8):1041-1051. doi:10.1038/s41556-019-0360-z
924 13. Sato T, Stange DE, Ferrante M, et al. Long-term expansion of epithelial organoids from
925 human colon, adenoma, adenocarcinoma, and Barrett's epithelium. *Gastroenterology*.
926 2011;141(5):1762-1772. doi:10.1053/j.gastro.2011.07.050

927 14. Fujii M, Matano M, Toshimitsu K, et al. Human Intestinal Organoids Maintain Self-Renewal
928 Capacity and Cellular Diversity in Niche-Inspired Culture Condition. *Cell Stem Cell*.
929 2018;23(6):787-793.e6. doi:10.1016/j.stem.2018.11.016
930 15. Fitzgerald HC, Dhakal P, Behura SK, Schust DJ, Spencer TE. Self-renewing endometrial
931 epithelial organoids of the human uterus. *Proc Natl Acad Sci U S A*. 2019;116(46):23132-
932 23142. doi:10.1073/pnas.1915389116
933 16. Nakamura T, Sato T. Advancing Intestinal Organoid Technology Toward Regenerative
934 Medicine. *CMGH*. 2018;5(1):51-60. doi:10.1016/j.jcmgh.2017.10.006
935 17. Cruz-Acuña R, Quirós M, Farkas AE, et al. Synthetic hydrogels for human intestinal
936 organoid generation and colonic wound repair. *Nat Cell Biol*. 2017;19(11):1326-1335.
937 doi:10.1038/ncb3632
938 18. Sato T, Vries RG, Snippert HJ, et al. Single Lgr5 stem cells build crypt-villus structures in
939 vitro without a mesenchymal niche. *Nature*. 2009;459(7244):262-265.
940 doi:10.1038/nature07935
941 19. Talbot NC, Caperna TJ. Proteome array identification of bioactive soluble proteins/peptides
942 in Matrigel: relevance to stem cell responses. *Cytotechnology*. 2015;67(5):873-883.
943 doi:10.1007/s10616-014-9727-y
944 20. Hughes CS, Postovit LM, Lajoie GA. Matrigel: a complex protein mixture required for
945 optimal growth of cell culture. *Proteomics*. 2010;10(9):1886-1890.
946 doi:10.1002/pmic.200900758
947 21. Cruz-Acuña R, García AJ. Synthetic hydrogels mimicking basement membrane matrices
948 to promote cell-matrix interactions. *Matrix Biol*. 2017;57-58:324-333.
949 doi:10.1016/j.matbio.2016.06.002
950 22. Capeling MM, Czerwinski M, Huang S, et al. Nonadhesive Alginate Hydrogels Support
951 Growth of Pluripotent Stem Cell-Derived Intestinal Organoids. *Stem Cell Reports*.
952 2019;12(2):381-394. doi:10.1016/j.stemcr.2018.12.001
953 23. Gjorevski N, Sachs N, Manfrin A, et al. Designer matrices for intestinal stem cell and
954 organoid culture. *Nat Publ Gr*. 2016;539(7630):560-564. doi:10.1038/nature20168
955 24. Kratochvil MJ, Seymour AJ, Li TL, Paşca SP, Kuo CJ, Heilshorn SC. Engineered materials
956 for organoid systems. *Nat Rev Mater*. 2019;4(9):606-622. doi:10.1038/s41578-019-0129-
957 9
958 25. Cook CD, Hill AS, Guo M, et al. Local remodeling of synthetic extracellular matrix
959 microenvironments by co-cultured endometrial epithelial and stromal cells enables long-
960 term dynamic physiological function. *Integr Biol (United Kingdom)*. 2017;9(4):271-289.

961 doi:10.1039/c6ib00245e
962 26. Hernandez-Gordillo V, Kassis T, Lampejo A, et al. Fully synthetic matrices for in vitro
963 culture of primary human intestinal enteroids and endometrial organoids. *Biomaterials*.
964 2020;254:120125. doi:10.1016/j.biomaterials.2020.120125
965 27. Arnold JT, Kaufman DG, Seppälä M, Lessey BA. Endometrial stromal cells regulate
966 epithelial cell growth in vitro: A new co-culture model. *Hum Reprod*. 2001;16(5):836-845.
967 doi:10.1093/humrep/16.5.836
968 28. Abbas Y, Brunel LG, Hollinshead MS, et al. Generation of a three-dimensional collagen
969 scaffold-based model of the human endometrium. *Interface Focus*. 2020;10(2):20190079.
970 doi:10.1098/rsfs.2019.0079
971 29. Osteen KG, Rodgers WH, Gaire M, Hargrove JT, Gorstein F, Matrisian LM. Stromal-
972 epithelial interaction mediates steroidal regulation of metalloproteinase expression in
973 human endometrium. *Proc Natl Acad Sci U S A*. 1994;91(21):10129-10133.
974 doi:10.1073/pnas.91.21.10129
975 30. Rezakhani S, Gjorevski N, Lutolf MP. Low-Defect Thiol-Michael Addition Hydrogels as
976 Matrigel Substitutes for Epithelial Organoid Derivation. *Adv Funct Mater*.
977 2020;30(48):2000761. doi:10.1002/adfm.202000761
978 31. Below CR, Kelly J, Brown A, et al. A microenvironment-inspired synthetic three-
979 dimensional model for pancreatic ductal adenocarcinoma organoids. *Nat Mater*. Published
980 online 2021. doi:10.1038/s41563-021-01085-1
981 32. Osteen KG, Hill GA, Hargrove JT, Gorstein F. Development of a method to isolate and
982 culture highly purified populations of stromal and epithelial cells from human endometrial
983 biopsy specimens. *Fertil Steril*. 1989;52(6):965-972. doi:10.1016/S0015-0282(16)53160-4
984 33. Turco MY, Gardner L, Hughes J, et al. Long-term, hormone-responsive organoid cultures
985 of human endometrium in a chemically defined medium. *Nat Cell Biol*. 2017;19(5):568-577.
986 doi:10.1038/ncb3516
987 34. Lutolf MP, Lauer-Fields JL, Schmoekel HG, et al. Synthetic matrix metalloproteinase-
988 sensitive hydrogels for the conduction of tissue regeneration: Engineering cell-invasion
989 characteristics. *Proc Natl Acad Sci U S A*. 2003;100(9):5413-5418.
990 doi:10.1073/pnas.0737381100
991 35. Cambria E, Renggli K, Ahrens CC, et al. Covalent Modification of Synthetic Hydrogels with
992 Bioactive Proteins via Sortase-Mediated Ligation. *Biomacromolecules*. 2015;16(8):2316-
993 2326. doi:10.1021/acs.biomac.5b00549
994 36. Kuhlman W, Taniguchi I, Griffith LG, Mayes AM. Interplay between PEO tether length and

995 ligand spacing governs cell spreading on RGD-modified PMMA-g-PEO comb copolymers.
996 *Biomacromolecules*. 2007;8(10):3206-3213. doi:10.1021/bm070237o
997 37. Wojtowicz AM, Shekaran A, Oest ME, et al. Coating of biomaterial scaffolds with the
998 collagen-mimetic peptide GFOGER for bone defect repair. *Biomaterials*. 2010;31(9):2574-
999 2582. doi:10.1016/j.biomaterials.2009.12.008
1000 38. Gao X, Groves MJ. Fibronectin-binding peptides. I. Isolation and characterization of two
1001 unique fibronectin-binding peptides from gelatin. *Eur J Pharm Biopharm*. 1998;45(3):275-
1002 284. doi:10.1016/S0939-6411(98)00010-1
1003 39. Johnson G, Moore SW. Identification of a structural site on acetylcholinesterase that
1004 promotes neurite outgrowth and binds laminin-1 and collagen IV. *Biochem Biophys Res*
1005 *Commun*. 2004;319(2):448-455. doi:10.1016/j.bbrc.2004.05.018
1006 40. Kurita T, Medina R, Schabel AB, et al. The activation function-1 domain of estrogen
1007 receptor α in uterine stromal cells is required for mouse but not human uterine epithelial
1008 response to estrogen. *Differentiation*. 2005;73(6):313-322. doi:10.1111/j.1432-
1009 0436.2005.00033.x
1010 41. Cunha GR, Baskin L. Use of sub-renal capsule transplantation in developmental biology.
1011 *Differentiation*. 2016;91(4-5):4-9. doi:10.1016/j.diff.2015.10.007
1012 42. Rawlings TM, Makwana K, Taylor DM, et al. Modelling the impact of decidual senescence
1013 on embryo implantation in human endometrial assembloids. *Elife*. 2021;10.
1014 doi:10.7554/eLife.69603
1015 43. Baugh LM, Goods BA, Gnecco JS, et al. Integrating endometrial proteomic and single cell
1016 transcriptomic pipelines reveals distinct menstrual cycle and endometriosis-associated
1017 molecular profiles. *medRxiv*. Published online January 1, 2022:2022.01.29.22269829.
1018 doi:10.1101/2022.01.29.22269829
1019 44. Käll L, Storey JD, Noble WS. Non-parametric estimation of posterior error probabilities
1020 associated with peptides identified by tandem mass spectrometry. *Bioinformatics*.
1021 2008;24(16):42-48. doi:10.1093/bioinformatics/btn294
1022 45. Oberg AL, Mahoney DW, Eckel-Passow JE, et al. Statistical analysis of relative labeled
1023 mass spectrometry data from complex samples using ANOVA. *J Proteome Res*.
1024 2008;7(1):225-233. doi:10.1021/pr700734f
1025 46. Ritchie ME, Phipson B, Wu D, et al. limma powers differential expression analyses for RNA-
1026 sequencing and microarray studies. *Nucleic Acids Res*. 2015;43(7):e47-e47.
1027 doi:10.1093/nar/gkv007
1028 47. Robinson MD, McCarthy DJ, Smyth GK. edgeR: A Bioconductor package for differential

1029 expression analysis of digital gene expression data. *Bioinformatics*. 2009;26(1):139-140.
1030 doi:10.1093/bioinformatics/btp616
1031 48. McCarthy DJ, Chen Y, Smyth GK. Differential expression analysis of multifactor RNA-Seq
1032 experiments with respect to biological variation. *Nucleic Acids Res*. 2012;40(10):4288-
1033 4297. doi:10.1093/nar/gks042
1034 49. Zhang Y, Parmigiani G, Johnson WE. ComBat-seq: batch effect adjustment for RNA-seq
1035 count data. *NAR Genomics Bioinforma*. 2020;2(3):1-10. doi:10.1093/nargab/lqaa078
1036 50. Wang W, Vilella F, Alama P, et al. Single-cell transcriptomic atlas of the human
1037 endometrium during the menstrual cycle. *Nat Med*. 2020;26(10):1644-1653.
1038 doi:10.1038/s41591-020-1040-z
1039 51. Lucas ES, Vrljicak P, Muter J, et al. Recurrent pregnancy loss is associated with a pro-
1040 senescent decidual response during the peri-implantation window. *Commun Biol*.
1041 2020;3(1):37. doi:10.1038/s42003-020-0763-1
1042 52. O'Connor BB, Pope BD, Peters MM, Ris-Stalpers C, Parker KK. The role of extracellular
1043 matrix in normal and pathological pregnancy: Future applications of microphysiological
1044 systems in reproductive medicine. *Exp Biol Med*. 2020;245(13):1163-1174.
1045 doi:10.1177/1535370220938741
1046 53. Aplin JD, Jones CJP. Extracellular Matrix in Endometrium and Decidua. In: Genbačev O,
1047 Klopper A, Beaconsfield R, eds. *Placenta as a Model and a Source*. Springer US;
1048 1989:115-128. doi:10.1007/978-1-4613-0823-2_12
1049 54. Aplin JD, Jones CJP. Extracellular Matrix in Endometrium and Decidua. In: Genbačev O,
1050 Klopper A, Beaconsfield R, eds. *Placenta as a Model and a Source*. Springer US;
1051 1989:115-128. doi:10.1007/978-1-4613-0823-2_12
1052 55. Gellersen B, Brosens JJ. Cyclic decidualization of the human endometrium in reproductive
1053 health and failure. *Endocr Rev*. 2014;35(6):851-905. doi:10.1210/er.2014-1045
1054 56. Béliard A, Donnez J, Nisolle M, Foidart JM. Localization of laminin, fibronectin, E-cadherin,
1055 and integrins in endometrium and endometriosis. *Fertil Steril*. 1997;67(2):266-272.
1056 doi:10.1016/S0015-0282(97)81909-7
1057 57. Bischof P, Redard M, Gindre P, Vassilakos P, Campana A. Localization of alpha 2, alpha
1058 5 and alpha 6 integrin subunits in human endometrium, decidua and trophoblast. *Eur J*
1059 *Obstet Gynecol Reprod Biol*. 1993;51(3):217-226. doi:10.1016/0028-2243(93)90038-E
1060 58. Puy LA, Pang C, Librach CL. Immunohistochemical analysis of alphavbeta5 and
1061 alphavbeta6 integrins in the endometrium and endometriosis. *Int J Gynecol Pathol Off J*
1062 *Int Soc Gynecol Pathol*. 2002;21(2):167-177. doi:10.1097/00004347-200204000-00010

1063 59. Tabibzadeh S. Patterns of expression of integrin molecules in human endometrium
1064 throughout the menstrual cycle. *Hum Reprod*. 1992;7(6):876-882.
1065 doi:10.1093/oxfordjournals.humrep.a137753
1066 60. Creus M, Balasch J, Ordi J, et al. Integrin expression in normal and out-of-phase
1067 endometria. *Hum Reprod*. 1998;13(12):3460-3468. doi:10.1093/humrep/13.12.3460
1068 61. Aplin JD, Spanswick C, Behzad F, Kimber SJ, Vićovac L. Molecular aspects of
1069 implantation: Integrins β5, β3 and αv are apically distributed in endometrial epithelium. *Mol*
1070 *Hum Reprod*. 1996;2(7):527-534. doi:10.1093/molehr/2.7.527
1071 62. Lessey BA, Damjanovich L, Coutifaris C, Castelbaum A, Albeida SM, Buck CA. Integrin
1072 adhesion molecules in the human endometrium. Correlation with the normal and abnormal
1073 menstrual cycle. *J Clin Invest*. 1992;90(1):188-195. doi:10.1172/JCI115835
1074 63. Lessey BA, Castelbaum AJ. Integrins and implantation in the human. *Rev Endocr Metab*
1075 *Disord*. 2002;3(2):107-117. doi:10.1023/a:1015450727580
1076 64. Casals G, Ordi J, Creus M, et al. Expression pattern of osteopontin and αvβ3 integrin during
1077 the implantation window in infertile patients with early stages of endometriosis. *Hum*
1078 *Reprod*. 2012;27(3):805-813. doi:10.1093/humrep/der432
1079 65. Coughlan C, Sinagra M, Ledger W, Li TC, Laird S. Endometrial integrin expression in
1080 women with recurrent implantation failure after in vitro fertilization and its relationship to
1081 pregnancy outcome. *Fertil Steril*. 2013;100(3):825-830.
1082 doi:10.1016/j.fertnstert.2013.05.007
1083 66. Garcia-Alonso L, Handfield L-F, Roberts K, et al. Mapping the temporal and spatial
1084 dynamics of the human endometrium in vivo and in vitro. *Nat Genet*. 2021;53(12):1698-
1085 1711. doi:10.1038/s41588-021-00972-2
1086 67. Lessey BA, Damjanovich L, Coutifaris C, Castelbaum A, Albelda SM, Buck CA. Integrin
1087 adhesion molecules in the human endometrium. Correlation with the normal and abnormal
1088 menstrual cycle. *J Clin Invest*. 1992;90(1):188-195. doi:10.1172/JCI115835
1089 68. Hynes RO. Integrins: Bidirectional, Allosteric Signaling Machines. *Cell*. 2002;110(6):673-
1090 687. doi:https://doi.org/10.1016/S0092-8674(02)00971-6
1091 69. Hehlgans S, Haase M, Cordes N. Signalling via integrins: implications for cell survival and
1092 anticancer strategies. *Biochim Biophys Acta*. 2007;1775(1):163-180.
1093 doi:10.1016/j.bbcan.2006.09.001
1094 70. Fields GB. Synthesis and biological applications of collagen-model triple-helical peptides.
1095 *Org Biomol Chem*. 2010;8(6):1237-1258. doi:10.1039/B920670A
1096 71. Carafoli F, Hamaia SW, Bihan D, Hohenester E, Farndale RW. An Activating Mutation

1097 Reveals a Second Binding Mode of the Integrin α2 I Domain to the GFOGER Motif in
1098 Collagens. *PLoS One*. 2013;8(7):e69833. https://doi.org/10.1371/journal.pone.0069833
1099 72. Khoshnoodi J, Pedchenko V, Hudson BG. Mammalian collagen IV. *Microsc Res Tech*.
1100 2008;71(5):357-370. doi:https://doi.org/10.1002/jemt.20564
1101 73. Gardner H. Integrin α1β1. *Adv Exp Med Biol*. 2014;819:21-39. doi:10.1007/978-94-017-
1102 9153-3_2
1103 74. Valdez J, Cook CD, Ahrens CC, et al. On-demand dissolution of modular, synthetic
1104 extracellular matrix reveals local epithelial-stromal communication networks. *Biomaterials*.
1105 2017;130:90-103. doi:10.1016/j.biomaterials.2017.03.030
1106 75. Soofi SS, Last JA, Lliensiek SJ, Nealey PF, Murphy CJ. Elastic modulus of Matrigel as
1107 determined by AFM. *J Struct Biol*. 2009;167(3):216-219.
1108 doi:10.1016/j.jsb.2009.05.005.The
1109 76. Abbas Y, Carnicer-Lombarte A, Gardner L, et al. Tissue stiffness at the human maternal-
1110 fetal interface. *Hum Reprod*. 2019;34(10):1999-2008. doi:10.1093/humrep/dez139
1111 77. Myers KM, Elad D. Biomechanics of the human uterus. *Wiley Interdiscip Rev Syst Biol*
1112 *Med*. 2017;9(5):1-20. doi:10.1002/wsbm.1388
1113 78. Wetendorf M, DeMayo FJ. The progesterone receptor regulates implantation,
1114 decidualization, and glandular development via a complex paracrine signaling network. *Mol*
1115 *Cell Endocrinol*. 2012;357(1-2):108-118. doi:10.1016/j.mce.2011.10.028
1116 79. Geisert R, Fazleabas A, Lucy M, Mathew D. Interaction of the conceptus and endometrium
1117 to establish pregnancy in mammals: role of interleukin 1β. *Cell Tissue Res*.
1118 2012;349(3):825-838. doi:10.1007/s00441-012-1356-1
1119 80. Critchley HO, Maybin JA, Armstrong GM, Williams ARW. Physiology of the endometrium
1120 and regulation of menstruation. *Physiol Rev*. Published online February 7, 2020.
1121 doi:10.1152/physrev.00031.2019
1122 81. Mehasseb MK, Panchal R, Taylor AH, Brown L, Bell SC, Habiba M. Estrogen and
1123 progesterone receptor isoform distribution through the menstrual cycle in uteri with and
1124 without adenomyosis. *Fertil Steril*. 2011;95(7):2228-2235, 2235.e1.
1125 doi:10.1016/j.fertnstert.2011.02.051
1126 82. Cunha GR, Bigsby RM, Cooke PS, Sugimura Y. Stromal-epithelial interactions in adult
1127 organs. *Cell Differ*. 1985;17(3):137-148. doi:10.1016/0045-6039(85)90481-6
1128 83. Cooke PS, Buchanan DL, Young P, et al. Stromal estrogen receptors mediate mitogenic
1129 effects of estradiol on uterine epithelium. *Proc Natl Acad Sci U S A*. 1997;94(12):6535-
1130 6540. doi:10.1073/pnas.94.12.6535

1131 84. Benjamini Y, Hochberg Y. Controlling the False Discovery Rate: A Practical and Powerful
1132 Approach to Multiple Testing. *J R Stat Soc Ser B*. 1995;57(1):289-300.
1133 doi:https://doi.org/10.1111/j.2517-6161.1995.tb02031.x
1134 85. Reavey JJ, Walker C, Nicol M, et al. Markers of human endometrial hypoxia can be
1135 detected in vivo and ex vivo during physiological menstruation. *Hum Reprod*.
1136 2021;36(4):941-950. doi:10.1093/humrep/deaa379
1137 86. Bruner KL, Rodgers WH, Gold LI, et al. Transforming growth factor β mediates the
1138 progesterone suppression of an epithelial metalloproteinase by adjacent stroma in the
1139 human endometrium. *Proc Natl Acad Sci U S A*. 1995;92(16):7362-7366.
1140 doi:10.1073/pnas.92.16.7362
1141 87. Goffin F, Munaut C, Frankenne F, et al. Expression pattern of metalloproteinases and
1142 tissue inhibitors of matrix-metalloproteinases in cycling human endometrium. *Biol Reprod*.
1143 2003;69(3):976-984. doi:10.1095/biolreprod.103.015933
1144 88. Curry TEJ, Osteen KG. The matrix metalloproteinase system: changes, regulation, and
1145 impact throughout the ovarian and uterine reproductive cycle. *Endocr Rev*.
1146 2003;24(4):428-465. doi:10.1210/er.2002-0005
1147 89. Large MJ, DeMayo FJ. The regulation of embryo implantation and endometrial
1148 decidualization by progesterone receptor signaling. *Mol Cell Endocrinol*. 2012;358(2):155-
1149 165. doi:10.1016/j.mce.2011.07.027
1150 90. Wang H, Critchley HO, Kelly RW, Shen D, Baird DT. Progesterone receptor subtype B is
1151 differentially regulated in human endometrial stroma. *Mol Hum Reprod*. 1998;4(4):407-
1152 412. doi:10.1093/molehr/4.4.407
1153 91. Kokawa K, Shikone T, Nakano R. Apoptosis in the human uterine endometrium during the
1154 menstrual cycle. *J Clin Endocrinol Metab*. 1996;81(11):4144-4147.
1155 doi:10.1210/jcem.81.11.8923873
1156 92. Armstrong GM, Maybin JA, Murray AA, et al. Endometrial apoptosis and neutrophil
1157 infiltration during menstruation exhibits spatial and temporal dynamics that are
1158 recapitulated in a mouse model. *Sci Rep*. 2017;7(1):17416. doi:10.1038/s41598-017-
1159 17565-x
1160 93. Miyoshi H, VanDussen KL, Malvin NP, et al. Prostaglandin E2 promotes intestinal repair
1161 through an adaptive cellular response of the epithelium. *EMBO J*. 2017;36(1):5-24.
1162 doi:10.15252/embj.201694660
1163 94. Wang Y, Nicholes K, Shih IM. The Origin and Pathogenesis of Endometriosis. *Annu Rev*
1164 *Pathol Mech Dis*. 2020;15:71-95. doi:10.1146/annurev-pathmechdis-012419-032654

1165 95. Vercellini P, Viganò P, Somigliana E, Fedele L. Endometriosis: Pathogenesis and
1166 treatment. *Nat Rev Endocrinol*. 2014;10(5):261-275. doi:10.1038/nrendo.2013.255
1167 96. Horne AW, Saunders PTK. SnapShot: Endometriosis. *Cell*. 2019;179(7):1677-1677.e1.
1168 doi:10.1016/j.cell.2019.11.033
1169 97. Bulun SE, Cheng Y-H, Yin P, et al. Progesterone resistance in endometriosis: Link to failure
1170 to metabolize estradiol. *Mol Cell Endocrinol*. 2006;248(1):94-103.
1171 doi:https://doi.org/10.1016/j.mce.2005.11.041
1172 98. Al-Sabbagh M, Lam EW-F, Brosens JJ. Mechanisms of endometrial progesterone
1173 resistance. *Mol Cell Endocrinol*. 2012;358(2):208-215.
1174 doi:https://doi.org/10.1016/j.mce.2011.10.035
1175 99. Zondervan KT, Becker CM, Missmer SA. Endometriosis. *N Engl J Med*.
1176 2020;382(13):1244-1256. doi:10.1056/NEJMra1810764
1177 100. Chung D, Gao F, Jegga AG, Das SK. Estrogen mediated epithelial proliferation in the
1178 uterus is directed by stromal Fgf10 and Bmp8a. *Mol Cell Endocrinol*. 2015;400:48-60.
1179 doi:10.1016/j.mce.2014.11.002
1180 101. Winuthayanon W, Lierz SL, Delarosa KC, et al. Juxtacrine Activity of Estrogen Receptor α
1181 in Uterine Stromal Cells is Necessary for Estrogen-Induced Epithelial Cell Proliferation. *Sci*
1182 *Rep*. 2017;7(1):8377. doi:10.1038/s41598-017-07728-1
1183 102. Wingfield M, Macpherson A, Healy DL, Rogers PA. Cell proliferation is increased in the
1184 endometrium of women with endometriosis. *Fertil Steril*. 1995;64(2):340-346.
1185 doi:10.1016/s0015-0282(16)57733-4
1186 103. Lenz J, Chvatal R, Fiala L, Konecna P, Lenz D. Comparative immunohistochemical study
1187 of deep infiltrating endometriosis, lymph node endometriosis and atypical ovarian
1188 endometriosis including description of a perineural invasion. *Biomed Pap Med Fac Univ*
1189 *Palacky, Olomouc, Czechoslov*. 2021;165(1):69-79. doi:10.5507/bp.2020.006
1190 104. Colón-Caraballo M, García M, Mendoza A, Flores I. Human Endometriosis Tissue
1191 Microarray Reveals Site-specific Expression of Estrogen Receptors, Progesterone
1192 Receptor, and Ki67. *Appl Immunohistochem Mol Morphol AIMM*. 2019;27(7):491-500.
1193 doi:10.1097/PAI.0000000000000663
1194 105. Kurita T, Young P, Brody JR, Lydon JP, O'Malley BW, Cunha GR. Stromal progesterone
1195 receptors mediate the inhibitory effects of progesterone on estrogen-induced uterine
1196 epithelial cell deoxyribonucleic acid synthesis. *Endocrinology*. 1998;139(11):4708-4713.
1197 doi:10.1210/endo.139.11.6317
1198 106. Griffith LG, Swartz MA. Capturing complex 3D tissue physiology in vitro. *Nat Rev Mol Cell*

1199 *Biol*. 2006;7(3):211-224. doi:10.1038/nrm1858
1200 107. Stejskalová A, Fincke V, Nowak M, et al. Collagen I triggers directional migration, invasion
1201 and matrix remodeling of stroma cells in a 3D spheroid model of endometriosis. *Sci Rep*.
1202 2021;11(1):4115. doi:10.1038/s41598-021-83645-8
1203 108. Kuperman T, Gavriel M, Gotlib R, et al. Tissue-engineered multi-cellular models of the
1204 uterine wall. *Biomech Model Mechanobiol*. Published online 2020. doi:10.1007/s10237-
1205 020-01296-6
1206 109. Park DW, Choi DS, Ryu H-S, Kwon HC, Joo H, Min CK. A well-defined in vitro three-
1207 dimensional culture of human endometrium and its applicability to endometrial cancer
1208 invasion. *Cancer Lett*. 2003;195(2):185-192. doi:10.1016/s0304-3835(03)00131-9
1209 110. Wiwatpanit T, Murphy AR, Lu Z, et al. Scaffold-Free Endometrial Organoids Respond to
1210 Excess Androgens Associated With Polycystic Ovarian Syndrome. *J Clin Endocrinol*
1211 *Metab*. 2020;105(3):769-780. doi:10.1210/clinem/dgz100
1212 111. Wendel JRH, Wang X, Smith LJ, Hawkins SM. Three-Dimensional Biofabrication Models
1213 of Endometriosis and the Endometriotic Microenvironment. *Biomedicines*. 2020;8(11).
1214 doi:10.3390/biomedicines8110525
1215 112. Fang S, McLean J, Shi L, Vink J-SY, Hendon CP, Myers KM. Anisotropic Mechanical
1216 Properties of the Human Uterus Measured by Spherical Indentation. *Ann Biomed Eng*.
1217 2021;49(8):1923-1942. doi:10.1007/s10439-021-02769-0
1218 113. Bigsby RM. Control of growth and differentiation of the endometrium: The role of tissue
1219 interactions. In: *Annals of the New York Academy of Sciences*. Vol 955. ; 2002:110-117.
1220 doi:10.1111/j.1749-6632.2002.tb02771.x
1221 114. Cooke PS, Buchanan DL, Young P, et al. Stromal estrogen receptors mediate mitogenic
1222 effects of estradiol on uterine epithelium. *Proc Natl Acad Sci U S A*. 1997;94(12):6535-
1223 6540. doi:10.1073/pnas.94.12.6535
1224 115. Bentin-Ley U, Pedersen B, Lindenberg S, Falck Larsen J, Hamberger L, Horn T. Isolation
1225 and culture of human endometrial cells in a three-dimensional culture system. *J Reprod*
1226 *Fertil*. 1994;101(2):327-332. doi:10.1530/jrf.0.1010327
1227 116. Bentin-Ley U, Lindenberg S, Horn T, Larsen JF. Ultrastructure of endometrial epithelial
1228 cells in a three-dimensional cell culture system for human implantation studies. *J Assist*
1229 *Reprod Genet*. 1995;12(9):632-638. doi:10.1007/BF02212588
1230 117. Bläuer M, Heinonen PK, Martikainen PM, Tomás E, Ylikomi T. A novel organotypic culture
1231 model for normal human endometrium: Regulation of epithelial cell proliferation by estradiol
1232 and medroxyprogesterone acetate. *Hum Reprod*. 2005;20(4):864-871.

1233 doi:10.1093/humrep/deh722
1234 118. García-Solares J, Dolmans MM, Squifflet JL, Donnez J, Donnez O. Invasion of human
1235 deep nodular endometriotic lesions is associated with collective cell migration and nerve
1236 development. *Fertil Steril*. 2018;110(7):1318-1327. doi:10.1016/j.fertnstert.2018.08.016
1237 119. González-Ramos R, Defrère S, Devoto L. Nuclear factor-kappaB: a main regulator of
1238 inflammation and cell survival in endometriosis pathophysiology. *Fertil Steril*.
1239 2012;98(3):520-528. doi:10.1016/j.fertnstert.2012.06.021
1240 120. Yoshinaga K, Davies C, White K, et al. Interdisciplinary collaborative team for blastocyst
1241 implantation research: inception and perspectives. *Am J Reprod Immunol*. 2014;71(1):1-
1242 11. doi:10.1111/aji.12173
1243 121. Brown A, He H, Trumper E, Valdez J, Hammond P, Griffith LG. Engineering PEG-based
1244 hydrogels to foster efficient endothelial network formation in free-swelling and confined
1245 microenvironments. *Biomaterials*. 2020;243:119921.
1246 doi:10.1016/j.biomaterials.2020.119921
1247 122. Sofman M, Brown A, Griffith LG, Hammond PT. A modular polymer microbead
1248 angiogenesis scaffold to characterize the effects of adhesion ligand density on angiogenic
1249 sprouting. *Biomaterials*. 2021;264:120231.
1250 doi:https://doi.org/10.1016/j.biomaterials.2020.120231
1251
1252
1253
1254
1255

1256 **5. Figure Legends**

1257

1258 **Figure 1. A tissue-inspired multi-omic approach elucidates the design parameters to**
1259 **engineer a fully synthetic PEG hydrogel for the endometrium.** (A) Representative histological
1260 hematoxylin and eosin (H&E) stained samples of the menstrual cycle phases. (B) Heatmap of
1261 proteomic analysis of the human endometrium showing ECM proteins (matrisome) across the
1262 menstrual cycle (n=11 donors). Box colors indicated ECM protein associations: green
1263 corresponds to collagens; red to fibronectin; and purple to laminins. (C) Dot plot analysis of
1264 specific integrins expression from single cell RNA-seq data (n = 6 donors, 6,659 cells).
1265 Examination of stromal and epithelial component integrin expression across the menstrual cycle
1266 (proliferative and secretory phases). Circle size and color indicate P-value and variation about the
1267 means of the average expression value for each integrin chain in all cells (D) Schematic of the
1268 overall strategy to design and fabricate a synthetic ECM for the endometrium. 8-arm 20kDa PEG
1269 macromers are functionalized with cell matrix binders (FN, B.M.), integrin adhesion peptides, and
1270 polymerized with a protease-labile crosslinker. Descriptive outline of the key peptides utilized in
1271 the synthetic ECM formulation.

1272

1273 **Figure 2. Dual integrin ligand functionalization in softer synthetic matrix regimes enhance**
1274 **EEOs generation.** (A) Biomechanical properties (elastic moduli, Pa, n=3 gels) of synthetic
1275 hydrogel formulations, where "soft" = 3wt% (~300 Pa), "stiff" = 5wt% (~2kPa) and "stiffest" = 7wt%
1276 (~6kPa). (B) Representative images of scEEO and morphology in stiff (5wt%) in soft (3wt%) PEG
1277 hydrogels functionalized with only GFOGER (3mM) compared to Matrigel. (C) Day-15 images of
1278 hydrogel formulations comparing adhesion peptides reveals that GFOGER is necessary to
1279 generate scEEOs. Dual-adhesion-peptide functionalization with GFOGER (1.5mM) and PHSN-
1280 K-RGD (1.5 mM) is sufficient for robust scEEO generation. (D) Time-lapse images of 10-day
1281 cultures of EEO derived from single cells in synthetic hydrogels (PEG 3wt%-MIX). (E)
1282 Quantification of the scEEO formation efficiency in synthetic hydrogels relative to Matrigel (N=8).
1283 (F) Quantification of the total lumenized EEO (>100 um diameter) count and EEO diameter
1284 distribution after 10 days in culture. (G) Characterization of EEO morphology and polarity of EEOs
1285 generated in synthetic ECM (3wt%-MIX) compared to Matrigel via immunofluorescent (IF)
1286 analysis of ECM deposition for laminin (LMN) and F-actin localization after 14 days of culture in
1287 soft (3%) PEG MIX hydrogel and in Matrigel. (H-I) Characterization of protein and transcriptomic
1288 expression of hormone receptors in EEOs generated in synthetic hydrogels. (H) Representative
1289 images of PGR staining countered stained with F-actin (green) and DAPI (nuclei) and (I) qPCR
1290 analysis of mRNA expression of PGR and ESR in EEOs treated with either E_2 (E) or E_2 + MPA
1291 (EP) for 14 days. Analysis compares ESR, PGR values relative to matching E treatment groups
1292 (control). Significance is indicated as *p<0.05, **p<0.01, ***p<0.001.

1293 **Figure 3. Development and characterization of a synthetic endometrial stromal cell culture.**
1294 (A) Schematic of the workflow for culturing ESCs in 3D using a synthetic hydrogel. (B) Maximum
1295 intensity projection images of F-actin (green) reveal ESC remodeling (cell elongation and
1296 dispersion) at day 7 of culture in stromal (serum containg) media impacted primarily by hydrogel
1297 stiffness (20X magnification) as quantified in (C). (D) Time-lapse images of embedded ESCs in
1298 synthetic matrix (PEG) compared to the natural-derivedhydrogels Collagen I (~4mg/mL) and
1299 Matrigel (8 mg/mL) allow for long-term stable cultures. Vimentin stain (red) of ESC morphology
1300 cultured in synthetic and natural hydrogels. IL-1β (1ng/mL) treated ESC in synthetic hydrogel
1301 provided as a control for inflamed morphology. (E) Brightfield images of stromal decidualization
1302 morphology in synthetic ECMs as a function of matrix stiffness (3wt%, 5wt% and 7wt% *MIX*) after
1303 14 days of EP treatment and in standard ESC media or EEO medium (see Methods). (F)
1304 Biochemical measurement of prolactin (PRL) in the spent media (EEO media) from 15-day

1305 cultures in (E) compared to standard 2D polystyrene cultures (N=4). (G) Represenatitive
1306 fluorescent staining of DNA synthesis (EdU incorporation for 24 hrs hrs prior to fixation at day 15
1307 as a function of simulated cycle phase and inflammation cue, IL-1β (H) Quantification of mean
1308 EdU^+ staining from cultures shown in (G) shows IL-1β suppresses DNA synthesis of ESCs (n=3)
1309 (I) Quantification of apoptosis (cleaved caspase-3^+) in ESC cells stimulated with homrone and IL-
1310 1β treatment groups at day 15 of culture relative to total nuclei count (N=3) (J) Inflammatory
1311 challenge with IL-1β significantly suppressed PRL secretion in ESC cultures (E+ = E + IL1β, PE+=
1312 PE+IL1β, W = hormone withdrawal) (N=6). Significance is indicated as *p<0.05, **p<0.01,
1313 ***p<0.001. Scale bars are 50 μm, unless otherwise noted.
1314
1315 **Figure 4. Establishment of a co-culture model recapitulates the molecular signature of the**
1316 **human menstrual cycle in vitro.** (A) Schematic and representative images of the co-cultures.
1317 EEOs (10 intact organoids/uL) and ESC (10k cells/uL) are expanded separately and embedded
1318 in the synthetic ECM, cultured as 3ul droplets and maintained for 15 days of culture. A dual-
1319 adhesion peptide synthetic ECM (3wt% 20kDa-PEG) functionalized with GFOGER (1.5mM) and
1320 PHSRN-K-RGD (1.5mM) supports the establishment of the EEOs and ESC co-culture model. (B)
1321 Representative 3D images of day-15 endometrial EEOs (EpCAM = green) and ESC (Vimentin =
1322 red) in the co-cultures (scale =100 um). (C) Schematic and timeframe of the idealized 28-day
1323 menstrual cycle in vivo. (D) Experimental design for the validation of the co-culture endometrial
1324 model. Treatment groups are designed to mimic the hormonal changes in the phases of the
1325 menstrual cycle, including a pharmacologic induction of the menstruation using a PGR antagonist
1326 (RU-486, 10uM). 'Inflamed' groups were co-treated with IL1β (1ng/mL) throughout the length of
1327 the experiment. (E-G) Transcriptomic (bulk RNAseq) analysis of the co-culture models (n= 7). (E)
1328 Gene ontology (GO) analysis of the top significantly enriched GO terms that are downregulated
1329 or upregulated in response to progestin treatment. Cocultures treated with E2 + MPA ("PE") have
1330 gene ontology (GO) expression profiles that align with the secretory phase of the menstrual cycle.
1331 GSEA analysis of hallmark pathway gene sets show pathway changes consistent with
1332 corresponding phases of the menstrual cycle. All images and transcriptomic analysis were
1333 performed on day-15 co-cultures in the synthetic 3wt% 20kDa-PEG-Mix hydrogels (N=8). Data is
1334 shown with the −log of their P values.

1335 **Figure 5. Functional validation of the co-culture model recapitulates morphologic and**
1336 **biochemical cycle-dependent reproductive processes.** (A) Representative histological (IF)
1337 characterization of the proliferative and secretory phases of the menstrual cycle in vivo reveals
1338 morphologic and biochemical changes. Vimentin (red), F-Actin (Green), DAPI (blue). (B)
1339 Characterization of the epithelial morphology in co-cultures at day 15 of culture by IF reveals
1340 glandular maturation and invagination of EEOs in response to progestin treatment groups. (C) IF
1341 staining of PAEP (glycodelin) in co-cultures recapitulates the epithelial secretory phenotype. (D)
1342 Stromal decidualization was assessed by measuring prolactin secretion in the medium across 15
1343 days of culture. PRL secretion is induced by PE treatment but suppressed in menses treatment
1344 group. (E) PGR staining in the co-cultures at day 15 of treatment. (F) Temporal profiles of
1345 decidualization normalized to fold change relative to day 0 were performed by measuring spent
1346 media (N=12) and can be suppressed by IL1β treatment (1 ng/mL, E+, PE+). (G-H) Cleaved
1347 caspase-3 (Casp-3) IF in the co-cultures as a marker of apoptosis (G) and quantified in as positive
1348 staining per organoid area (H). All images are of day-15 co-cultures in the synthetic ECM 3wt%
1349 20kDa-PEG-Mix hydrogels. Significance is indicated as *p<0.05, **p<0.01, ***p<0.001.

1350 **Figure 6. Functional analysis of inflammatory cue (IL-1β) repsonses in co-cultures in**
1351 **synthetic hydrogel reveals the intitiation of the endometriotic phenotype mediated by cell-**
1352 **cell communication.** (A) 3D maximum intensity projections of PGR expresison in E2-only treated
1353 co-cultures in response to IL-1β stimulation (B-C) IL-1β stimulation (1 ng/mL) induces

1354 morphological changes in EEOs. Representative IF images (B) and quantification (C) of epithelial
1355 height (distance from base to apical edge of the epithelium, N=3). (D) Schematic of donor
1356 matched EEO monoculture and co-culture in IL-1β treatment groups. (E) Represenative images
1357 of time-lapse co-cultures stimulated with IL-1β reveals enlarged EEO diameter by day 7 of culture.
1358 (F) Quantication of the mean fold-change of EEO diameter across 15-days of cultures from daily
1359 time-lapse images in co-cultures (black) and monocultures (red) across treatment conditions (E,
1360 PE, W) and IL-1β-treated (E+, PE+) groups. Fold-change denotes the mean increase in diamter
1361 relative to day 1 of culture. Analysis compares the mean EEO growth rate between monoculture
1362 vs coculture (n=4; E + IL-1 p=0.0076; PE + IL-1β p=0.0026). (G) Immunostaining analysis of DNA
1363 synthesis in co-cultures and EEO monocultures by EdU incorporation in response to hormones
1364 and IL-1β treatment (N=3). (H-I) Quantification of proliferative profiles calculated as the number
1365 of EdU^+ cells per organoid area (mm^2) in (H) organoid monocultures and (I) co-cultures. (J)
1366 Working model of the cellular mechanisms driving epithelial and stromal communication in the
1367 endometrium under physiologic (hormones) and pathogenic (IL-1β -treated) conditions. All
1368 images are of day-15 co-cultures in the synthetic ECM 3wt% 20kDa-PEG-MIX hydrogels.
1369 Significance is indicated as *p<0.05, **p<0.01, ***p<0.001.

6. Supplementary Figures Legends:

Supplementary Fig 1. Characterization of the human endometrium using single cell transcriptomic analysis of the endometrium. (A) Expression of all integrin chains across the cycle for diverse subpopulations of endometrial cells (N=6); integrin β3 was not detected. (B) Violin plots of the integrin expression across the endometrial cell populations (N=6). (C) Validation of cell specific integrin expression in cultured endometrial cells. ESC and EEOs were cultured in 2D polystyrene (ESC) and in Matrigel (EEO) respectively and analyzed by qPCR for integrins relative to GAPDH (N=5). Significance is indicated as *p<0.05, **p<0.01, ***p<0.001.

Supplementary Fig 2. Workflow for EEO generation, hydrogel generation and screening. (A) Schematic of primary endometrial tissue processing workflow to generate organoids (B) Schematic of detailed EEO generation and hydrogel screening protocols.

Supplementary Fig 3. Screening and quantification of EEO generation in synthetic matrices across donors. Representative brightfield images of scEEO expansion comparing 3 different donors at day 7 cultured in either Matrigel or one of 4 different hydrogel formulations.

Supplementary Fig 4. Matrix stiffness affects EEO morphology. (A) Represenative brightfield images of day-14 scEEO morphology donors cultured in hydrogel formulations of GFOGER (3mM) or MIX (1.5 mM GFOGER, 1.5 mM PHSRN-K-RGD) in varying stiffnesses (3wt%, 5wt% and 7wt%). (B) Quantification of meandering phenotype as a percentage of EEOs confering a meandering phenotype (N = 4 biological replicates). (C) Representative maximum intensity projection and orthogonal view of scEEOs in Matrigel, soft PEG MIX gel, and stiff PEG MIX gel, stained for F-Actin (green).

Supplementary Figure 5. Comparative phenotype, proliferative activity and heterogenity of EEOs cultured in PEG vs Matrigel. (A) Representative image of F-actin stained scEEO derived in soft synthetic matrices compared to Matrigel at day 14 reveal a comparable rounded spherical morpholgy. (B) EpCAM staining of scEEOs confirms epithelial-origin in synthetic matrices and in Matrigel. (C) Ki67 staining of EEOs cultured in synthetic ECM and in Matrigel. (D) Image captures from videos reflect epithelial heterogeneity and motile cilia. EEOs cultured in synthetic matrices and stained for acetylated a-tubulin (red) reveal multi-ciliated and primary ciliated cells.

Supplementary Fig 6. Inflammation disrupts ESC morphology. (A) Representative brightfield images of ESC monocultures in response to inflammatory cue (IL-1β, 1 ng/mL), reveals increased elongation suggestive of a more active and motile phenotype. (B-C) Imaging and quantification of increased ESC remodeling capacity. (B) Immunofluorescent characterization of F-actin confirms morphogenic changes associated with response to IL-1β treatment (4X). Single cell segmentation (False colored red, 20X) cells elucidates the elongated morphologic changes associated with hormone treatment and IL-1β treatment in 3D (N=3). (C) Quantifaction of mean stromal cell surface area (N=3).

Supplementary Fig 7. Estimating cell ratios ex vivo for tissue modeling in vitro. 3D imaging of endometrial tissue biopsies using tissue clearing methods and confocal imaging were analyzed using the Imaris (Bitmap 9.6.0) software to segment the epithelial and stromal compartments of the native endometrium (n=3 donors; prolifertive n=2, secretory n=1; 3 different volumes) using the 'Surface' function to masks individual cell regions in a volumetric image. (A) The 'Cells' function Single cell segmentation tools from the software were used to calculate the number of epithelial cells (Epi) per volume of epithelial glands (Epi/μL). (B) ESC single cell counting in 3D was performed using the 'Spots' function by labeling and counting the DAPI+ nuclei in the image.

This estimations is calculated as the stroma, including other cellular components including the vascular and immune components. A similar approach was taken for co-culture in the *in vitro* models. (C) Cell concentration per unit area the native endometrium and the cell ration between epithelial cells and stromal cells. (D) 3D analysis of EEOs cultured in the synthetic matrices. (E) Cell density in vivo and in vitro comparing relative numbers and epithelial cell gland volumes. (F) No significant differences in the ratio between single ESCs concentration (ESC/µl) and Epithelial volume (gland/volume ratio).

Supplementary Fig 8. Establishment and transcriptomic analysis of monocultures and co-cocultures. (A) Representative brightfield images of co-culture (N=7) and monocultures of EEOs (N=1) and ESCs (N=6). (B) Unsupervised PCA analysis of bulk RNAseq show that day-15 co-cultures and monocultures cluster by culture type. Ellipses bound the 95% confidence interval for each group. (C) Plotting $log_2(fold\ change)$ against -$log_{10}(P\ value)$ in a volcano plot shows differentially expressed genes in cocultures as compared to cultures of ESC only.

Supplementary Fig 9. Trancriptomic evaluation of endometrial co-culture models of the menstrual cycle phases. (A) Hierarchical clustering heatmap of genes associated with the human menstrual cycle clusters samples based on hormone treatment groups in the co-cultures. Data is derived from 2 biological replicates (donors) that were maintained in nEEO media (B) Examination gene network analysis of the most significant up-and-down regulated GO associated genes.

Supplementary Fig 10. Functional and trancriptomic evaluation of endometrial co-culture recapitulation of the menstrual cycle phases. (A) Morphological assessment of altered cellular response to hormones and to inflammation (IL1β, 1ng/mL). Additional representative images of F-actin staining in EEO (green) and ESC (faux colored, orange) in co-culture under 'proliferative (E)' and 'secretory (PE)' hormone treatment groups for both EEOs and ESC. (B) Low-magnfication (4X) immunofluorescent staining of PAEP of the day-15 co-cultures reveals progesterone-induced secretory phenotype in the EEOs. (C) Transcriptomic analysis of MMP expression reveals differential expression patterns in response to hormone treatments. (D-E) Gene Set Enrichment Analysis (GSEA) on a ranked list of genes from a generalized linear model of the coculture bulk RNAseq data comparing different treatment groups. Hallmark pathways show gene expression changes consistent with corresponding phenotypic changes across the phases of the menstrual cycle.

Supplementary Fig 11. Apoptosis is increased in the menstrual phase and with IL-1β treament in the co-culture model (A) Comparison of apoptotic marker expression (cleaved caspase-3) immunofluorescent staining in co-cultures at day 15 in the menstrual cycle and inflamed groups in low (4X) magnification. E = estradiol only, PE = E + MPA, M = PE withdrawal + RU486), E+ = E + IL1β, and PE+ = PE+IL1β, M+ = M + IL-1β.

Supplementary Fig 12. Cell viability is decreased in the IL-1β treatment group in the co-culture models at day 15 in the 3% PEG MIX hydrogel. Low (4X, scale bar = 100 ums) and high (10X, scale bar = 50 ums) magnification of the Live (green) and Dead (red) assay in the hormone and IL-1β-treated groups comparing (A) ESC monocultures and (B) co-cultures in 3 ul droplet cultures.

Supplementary Fig 13. Co-cultures treated with IL-1β have transcriptomic profiles consistent with inflamed endometrial states. Co-cultures treated with IL-1β have transcriptomic profiles consistent with inflamed endometrial states. (A) A volcano plot of $log_2(fold\ change)$ against -$log_{10}(P\ value)$ for cocultures treated with the inflammatory cue (IL-1β, 1 ng/mL) as compared to non-inflamed controls. Transcript data is modeled using a

generalized linear model (see Methods) to account for inter-donor and hormone treatment variability. (B) A closer examination of the most significant GO terms reveals that canonical inflammatory genes are upregulated while PRL is downregulated, as expected for an inflamed environment. (C) Differentially expressed genes were analyzed using gene ontology (GO) analysis to examine the most up- and down- regulated biological processes upon IL1β treatment.

Supplementary Fig 14. Temporal evaluation of inflammatory response of co-cultures via targeted proteomics. Represenative co-culture (N=1 donor) of measured multiplex 45-panel of secreted cytokines measured in co-cultures throughout the 15-day experiment. Readings were measured every 3 days in control or IL-1β-treated conditions (N=3 technical replicates per day). (A) Luminex panel of up regulated and downregulated cytokines in response to IL-1β-treatment (representative results shown for day 15; similar data obtained for all conditions and time points). (B) Principal component analysis (PCA) and corresponding loading plots illustrate separation of culture conditions. (C) Profiles of MMP release into the medium in co-cultures. All images are of day-15 co-cultures in the synthetic ECM (3wt%-MIX). (E = estradiol only, PE = E + MPA, M = PE withdrawal + RU486), E+ = E + IL1β, and PE+ = PE+IL1β, M+ = M + IL-1β).

Supplementary Fig 15. Inflammatory stimuli alter stromal morphology in endometrial co-culture. (A) Representative brightfield image of ESC laden region in the co-culture in the PE treated groups stimulated with and without IL-1β at day 10 of culture in EEO co-culture media (B) IL-1β treated stromal cells revealed increased spindle morphology in co-cultures as stained for vimentin (red).

Supplementary Fig 16. Cell nuclei spacing and cell density in the organoid surface is comparable across treatment group conditions. A) Quantification of spacing between nuclei in optical sections of the organoids (left) and representative images of treatment groups (right), (N=3 donors). (B) Representative 3D image projection of nuclei distribution of organoids in the treatment groups. Nuclei density quantificaiton of per organoid surface area is comparable between treatment conditions. Image analysis was performed with Imaris software (N=3).

Supplementary Fig 17. Quantitative assesment of individual EEO diamater growth rates in in co-cultures and monocultures across 15-days of culture. Daily images were analyzed to quantify the diameter fold change of the organoids relative to day 1 of cultures. (A) Mean EEO growth rates of co-cultures and EEO only conditions across 15 days of culture (B) Analysis of individual day differences between donor matched co-culture (N=4) and monoculture (N=4) for all treatment groups. Data are mean ± SEM of 4 matched replicates. Signficance is indicated as *$p<0.05$, **$p<0.01$, ***$p<0.001$.

Supplementary Fig 18. EEOs can be generated and expanded directly into synthetic ECM from primary tissues. (A) Schematic of epithelial gland collection and EEO generation and expansion using synthetic matrix with Matrigel controls in parallel as a benchmark. (B) Brightfield images of EEOs generated in the synthetic matrix (3wt%-MIX) directly from freshly isolated gland fragments. (C) Characterization of Matrigel-free EEOs and immunofluorescent images of actin (green) staining. (D) Illustration of expansion and passaging of EEOs (p1) using the synthetic matrix.

Supplementary Fig 19. Trancriptomic evaluation of culture media effect on endometrial co-culture. (A) Hierarchical clustering heatmap of genes associated with the human menstrual cycle clusters samples based on hormone treatment groups in the co-cultures in 5 biological replicates (donors) that were maintained in 'EEO' media.

1509 **Supplementary Fig 20. Histological characterization of endometrial tissues collected.**
1510 Hematoxylin and eosin stain (H&E) of endometrial tissue from endometrial donors.
1511
1512 **Supplementary Fig 21. Synthetic matrix enables modeling of endometrial morphogenesis.**
1513 (A) Schematic of the endometrial architecture capturing the glandular (GE) and luminal (LE)
1514 epithelium. Experimental workflow of organoid morphogenic events that lead to the generation of
1515 glandular-monolayer structures in the synthetic matrix (3wt% PEG-MIX). (B) Schematic and
1516 representative images of the sections of the endometrial luminal and glandular epithelium.
1517 Immunofluorescent images of the monolayer section (Luminal epithelium, top) and the organoid
1518 section (gladular epitheliumm bottom). Cells are stained for Laminin (white), Dapi (blue), F-Actin
1519 (green). (C) Orthogonal view projections of z-stack images of the monolayers generated in
1520 traditional 2D polystyrene plates (left) and in the synthetic gels (right) reveals a columnar epithelial
1521 morphology in the gel monolayer compared to the 2D where the cells have lost their architecture.
1522 Cells are stained for F-Actin (green) and DAPI (blue).
1523
1524 **Table 1. Metadata of endometrial tissue donors.** Table outlining patient metadata and tissue
1525 processing.
1526
1527 **Video 1A: Beating multi-cilliated cells are visible in endometrial organoids cultured in**
1528 **Matrigel.** Live recording of beating cilia in organoids cultured in Matrigel at day 6 of culture
1529 estrogen (E) treatment groups. Recoding was acquired with a Keyence BZ-X800 Fluorescence
1530 Microscope recording option at 40X magnification.
1531
1532 **Video 1B: Beating multi-cilliated cells are visible in endometrial organoids cultured in**
1533 **synthetic hydrogels.** Live recording of beating cilia in organoids cultured in synthetic matrix
1534 (3wt%-*MIX*) at day 6 of culture estrogen (E) treatment groups. Recoding was acquired with a
1535 Keyence BZ-X800 Fluorescence Microscope recording option at 40X magnification.
1536
1537 **Video 2: Immuno-stained 3D rendering of proliferative phase treated organoid co-culture.**
1538 Representative 3D visualization of a z-stack (~635 um thickness) section of the stained
1539 endometrial co-culture in the synthetic ECM (3wt%-*MIX*) at day-15 of culture in the 'proliferative'
1540 treatment group. Images were captured using a ZEISS confocal Laser Scanning Microscope
1541 (LSM 880). 3D renderings were performed using Imaris (Bitmap 9.6.0) software to segement the
1542 organoids. Epithelium is stained for F-actin (green) and stroma stained for vimentin (red). DAPI
1543 was used as a counter stain for the nuclei.
1544
1545 **Video 3A: Time-lapse imaging of the endometrial co-culture in the 'proliferative'**
1546 **treatment group.** Representative (donor 259) brightfield time-lapse of endometrial co-culture in
1547 the synthetic hydrogel across 15 days of culture in the 'proliferative' (E) treatment group. Images
1548 were taken daily at 4X magnification with a Keyence BZ-X800 Fluorescence Microscope.
1549
1550 **Video 3B: Time-lapse imaging of the endometrial co-culture in the 'proliferative + IL1β'**
1551 **treatment group.** Representative (donor 259) brightfield time-lapse of endometrial co-culture in
1552 the synthetic hydrogel across 15 days of culture in the 'proliferative' + IL1β (E+) treatment
1553 group. Images were taken daily at 4X magnification with a Keyence BZ-X800 Fluorescence
1554 Microscope.

Video 3C: Time-lapse imaging of the endometrial co-culture in the 'secretory' treatment group. Representative (donor 259) brightfield time-lapse of endometrial co-culture in the synthetic hydrogel across 15 days of culture in the 'secretory' (PE) treatment group. Images were taken daily at 4X magnification with a Keyence BZ-X800 Fluorescence Microscope.

Video 3D: Time-lapse imaging of the endometrial co-culture in the 'secretory+ IL1β' treatment group. Representative (donor 259) brightfield time-lapse of endometrial co-culture in the synthetic hydrogel across 15 days of culture in the 'secretory' + IL1β (PE+) treatment group. Images were taken daily at 4X magnification with a Keyence BZ-X800 Fluorescence Microscope.

Video 3E: Time-lapse imaging of the endometrial co-culture in the 'menses' treatment group. Representative (donor 259) brightfield time-lapse of endometrial co-culture in the synthetic hydrogel across 15 days of culture in the 'menses' treatment group. Images were taken daily at 4X magnification with a Keyence BZ-X800 Fluorescence Microscope.

Video 3F: Time-lapse imaging of the stromal monoculture in the 'proliferative' treatment group. Representative (donor 259) brightfield time-lapse of endometrial ESC monoculture in the synthetic hydrogel across 15 days of culture in the 'proliferative' (E) treatment group. Images were taken daily at 4X magnification with a Keyence BZ-X800 Fluorescence Microscope.

Video 3G: Time-lapse imaging of the stromal monoculture in the 'proliferative + IL1β' treatment group. Representative (donor 259) brightfield time-lapse of endometrial ESC monoculture in the synthetic hydrogel across 15 days of culture in the 'proliferative' + IL1β (E+) treatment group. Images were taken daily at 4X magnification with a Keyence BZ-X800 Fluorescence Microscope.

Video 3H: Time-lapse imaging of the stromal monoculture in the 'secretory' treatment group. Representative (donor 259) brightfield time-lapse of endometrial ESC monoculture in the synthetic hydrogel across 15 days of culture in the 'secretory' (PE) treatment group. Images were taken daily at 4X magnification with a Keyence BZ-X800 Fluorescence Microscope.

Video 3I: Time-lapse imaging of the stromal monoculture in the 'secretory+ IL1β' treatment group. Representative (donor 259) brightfield time-lapse of endometrial ESC monoculture in the synthetic hydrogel across 15 days of culture in the 'secretory' + IL1β (PE+) treatment group. Images were taken daily at 4X magnification with a Keyence BZ-X800 Fluorescence Microscope.

Video 3J: Time-lapse imaging of the stromal monoculture in the 'menses' treatment group. Representative (donor 259) brightfield time-lapse of endometrial ESC monoculture in the synthetic hydrogel across 15 days of culture in the 'menses' treatment group. Images were taken daily at 4X magnification with a Keyence BZ-X800 Fluorescence Microscope.

Video 4A: Time-lapse imaging of the EEO monoculture in the 'secretory+ IL1β' treatment group. Representative (donor 272) brightfield time-lapse of endometrial EEO monoculture in the synthetic hydrogel across 15 days of culture in the 'secretory' + IL1β (PE+) treatment group. Images were taken daily at 4X magnification with a Keyence BZ-X800 Fluorescence Microscope.

1605 **Video 4B: Time-lapse imaging of the ESC monoculture in the 'secretory+ IL1β' treatment**
1606 **group.** Representative (donor 272) brightfield time-lapse of endometrial ESC monoculture in the
1607 synthetic hydrogel across 15 days of culture in the 'secretory' + IL1β (PE+) treatment group.
1608 Images were taken daily at 4X magnification with a Keyence BZ-X800 Fluorescence
1609 Microscope.
1610
1611 **Video 4C: Time-lapse imaging of the endometrial co-culture in the 'secretory+ IL1β'**
1612 **treatment group.** Representative (donor 272) brightfield time-lapse of endometrial co-culture in
1613 the synthetic hydrogel across 15 days of culture in the 'secretory' + IL1β (PE+) treatment group.
1614 Images were taken daily at 4X magnification with a Keyence BZ-X800 Fluorescence
1615 Microscope.

Graphical abstract

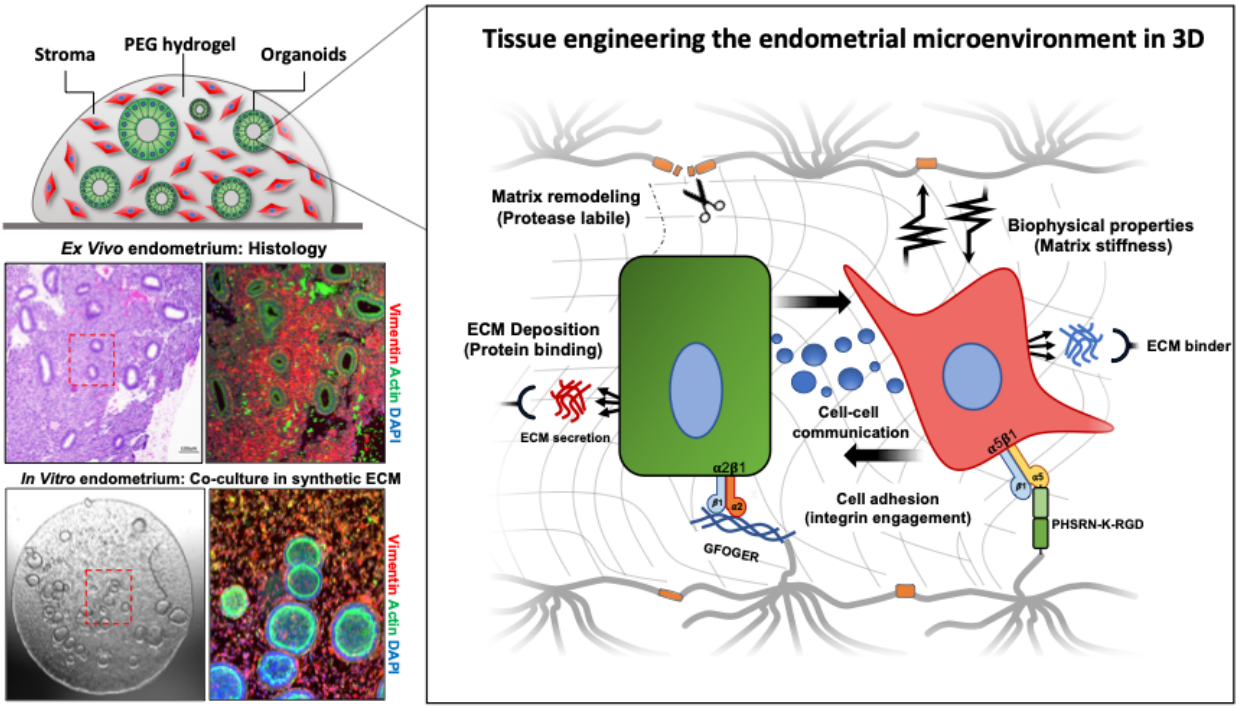

Figure 1. A tissue-inspired multi-omic approach elucidates the design parameters to engineer a fully synthetic PEG hydrogel for the endometrium.

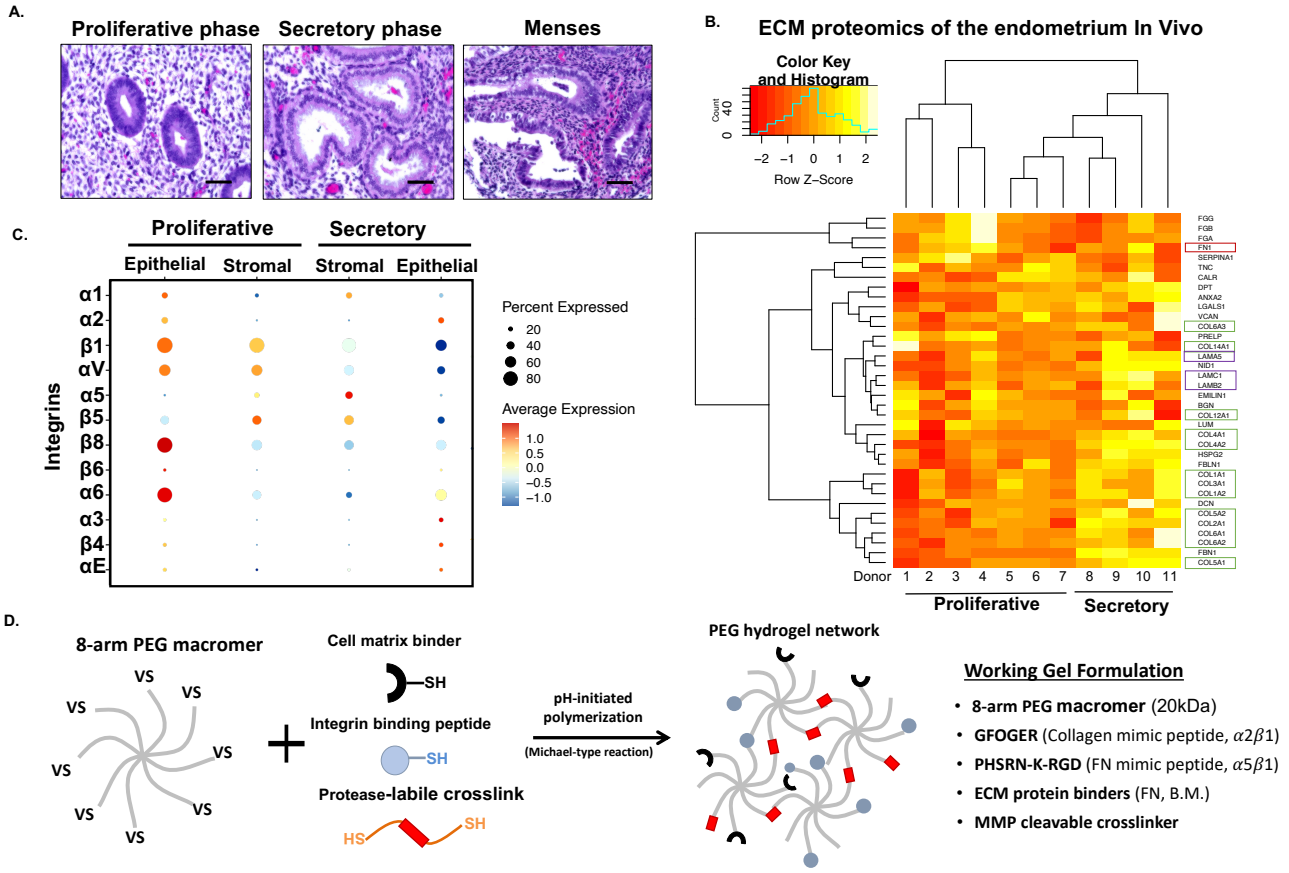

Figure 2. Dual integrin ligand peptide functionalization and softer synthetic matrix regimes enhance EEOs generation.

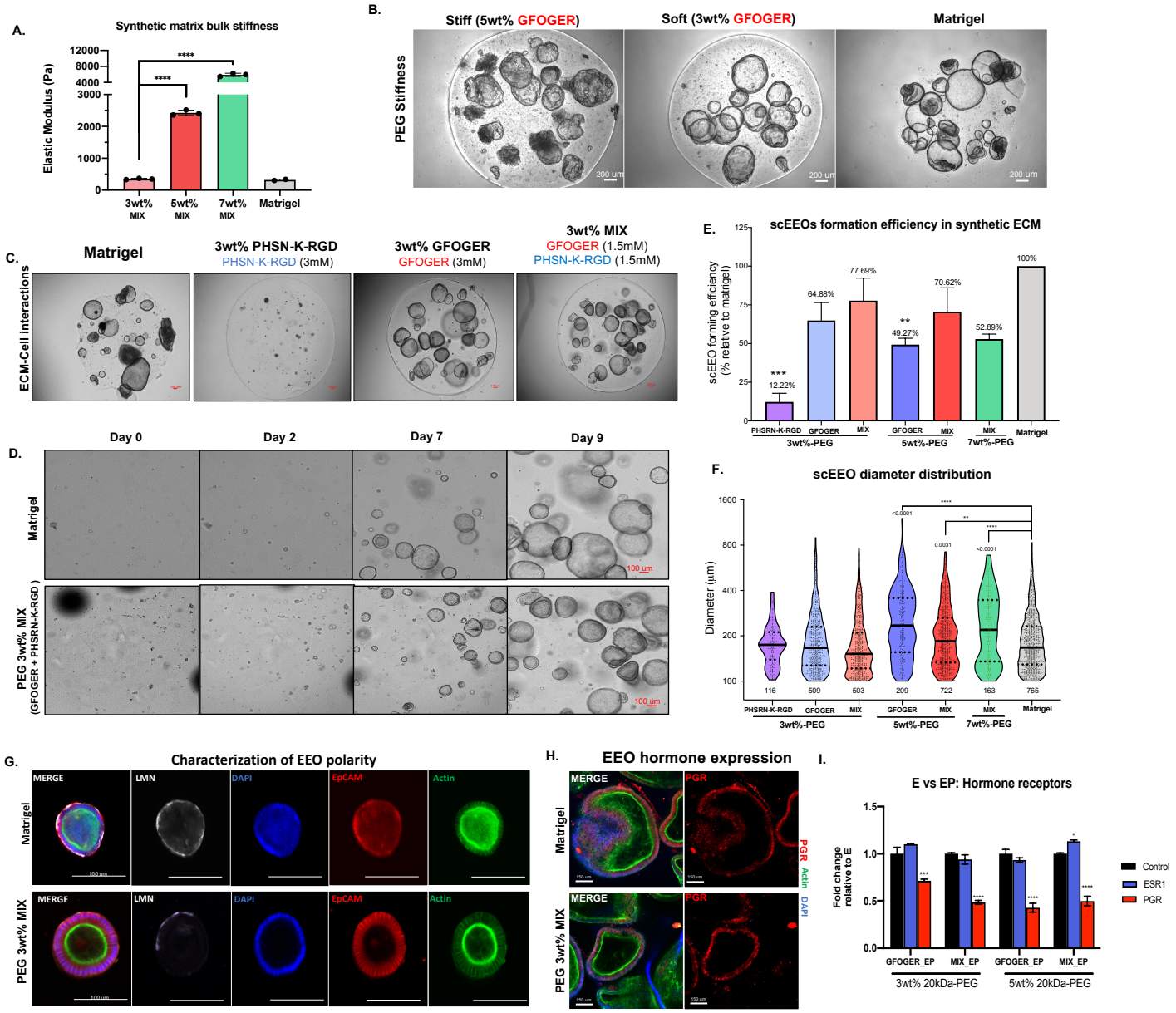

Figure 3. Development and characterization of a synthetic endometrial stromal cell culture.

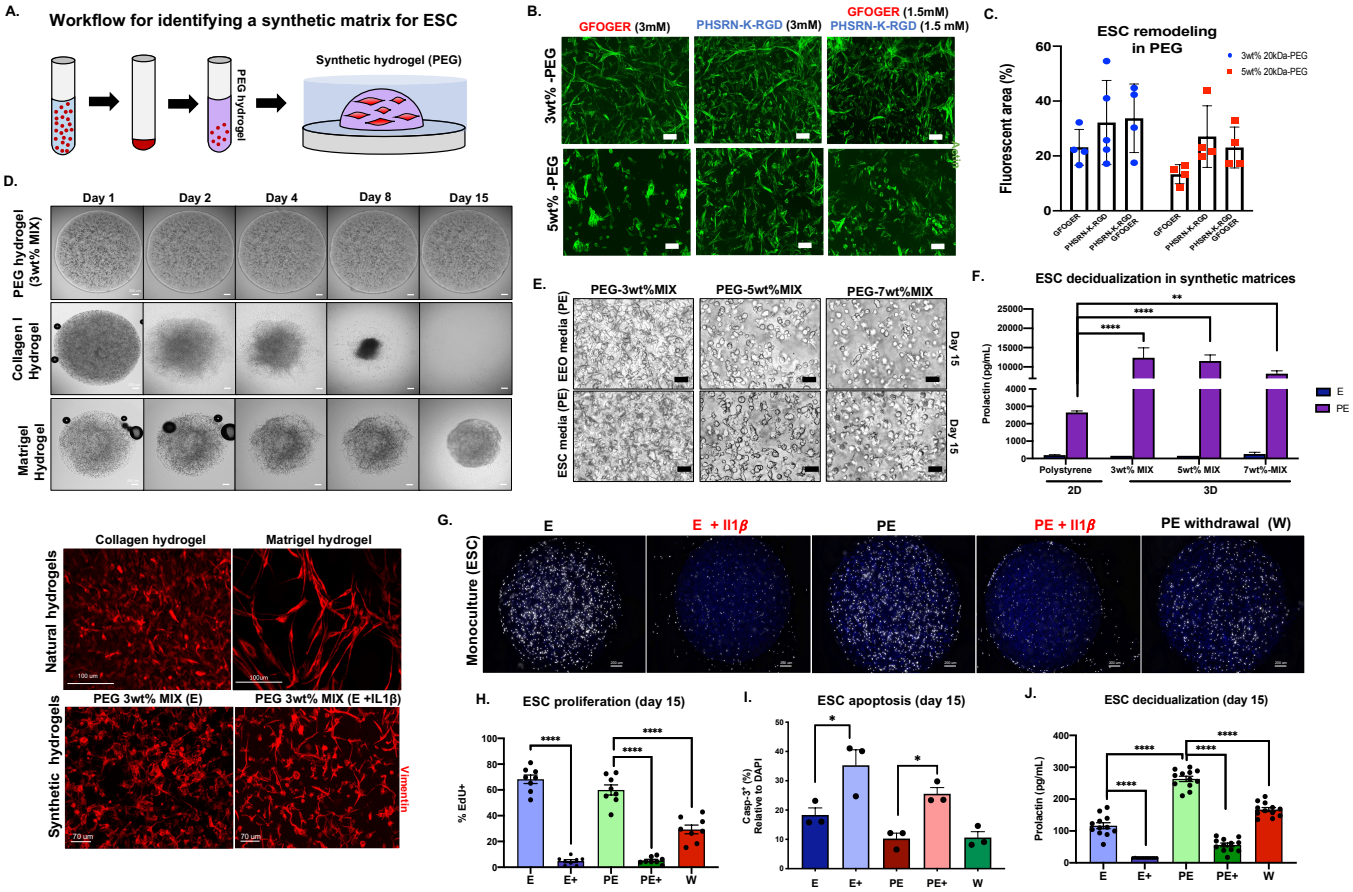

Figure 4. Establishment of a co-culture model recapitulates the molecular signature of the human menstrual cycle in vitro.

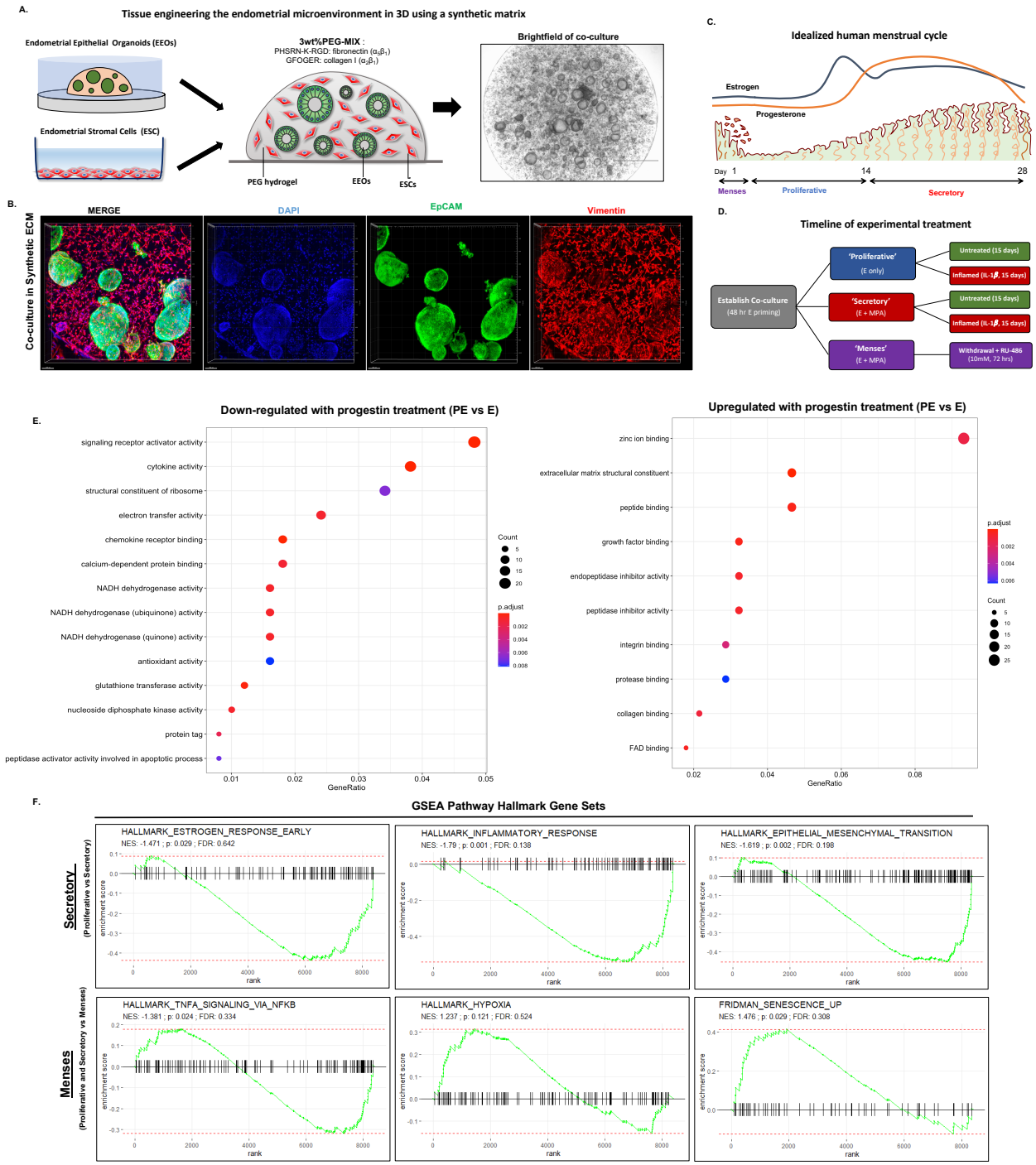

Figure 5. Functional validation of the co-culture model recapitulates menstrual cycle-relevant reproductive processes.

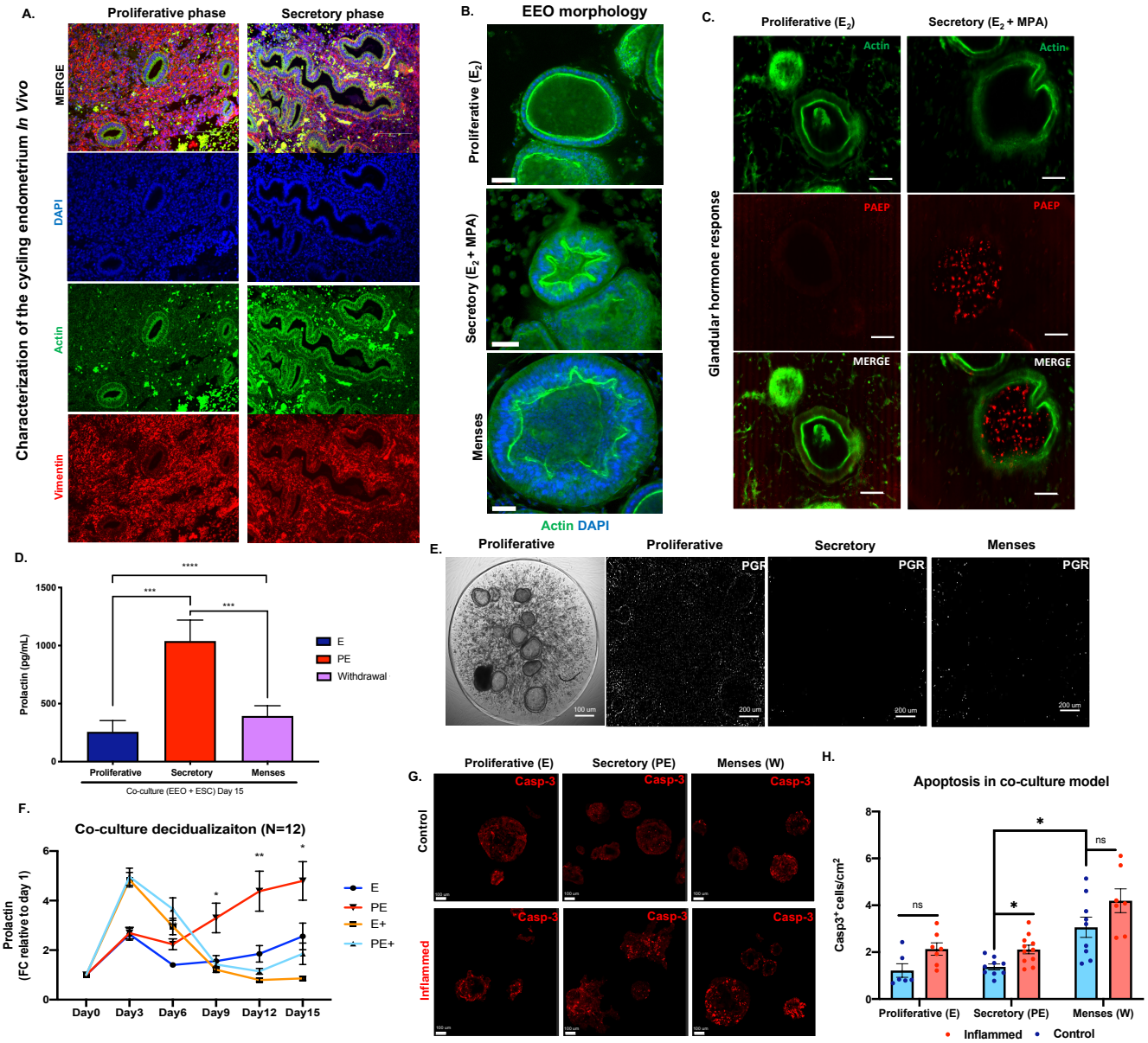
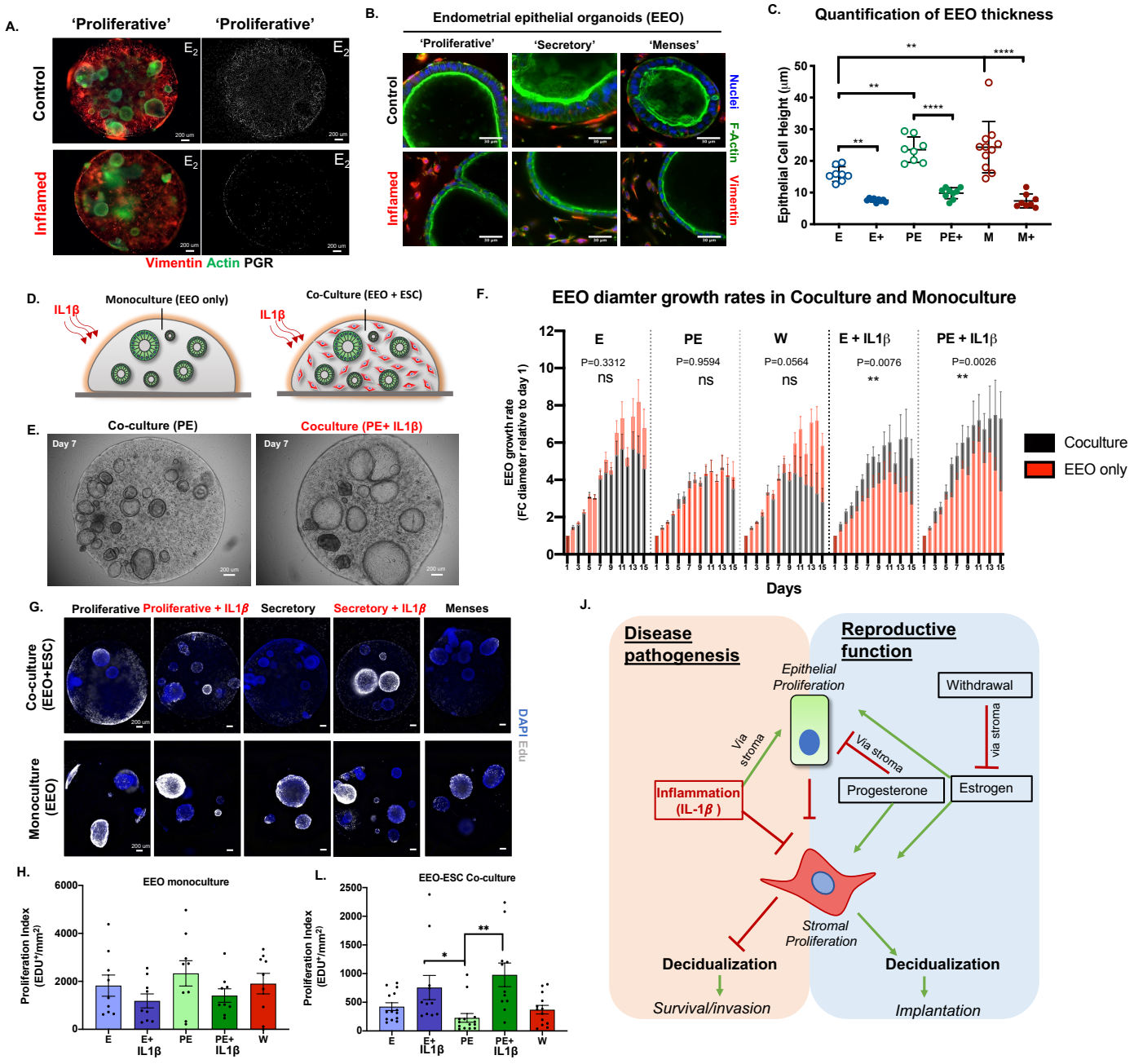
Figure 6. Functional analysis of inflammation in co-cultures in synthetic hydrogel reveals an endometriotic phenotype mediated by cell-cell communication.